Macromolecules

pubs.acs.org/Macromolecules Article

Interplay of Polymer Structure, Solvent Ordering, and Charge Fluctuations in Polyelectrolyte Solution Thermodynamics

Michael Beckinghausen and Andrew J. Spakowitz*

Cite This: *Macromolecules* 2023, 56, 136−152 Read Online

ACCESS | Metrics & More | Article Recommendations

ABSTRACT: We develop a polymer field-theoretic model that incorporates explicit treatment of semiflexibility and polar solvents, providing a framework to determine the impact of solvent ordering and concentration fluctuations on the thermodynamic behavior of polyelectrolyte solutions. We study the effect of dipole ordering on the electrostatic potential near a charged surface and the phase behavior of oppositely charged symmetric polyelectrolytes. The phase diagrams, incorporating quadratic-order concentration fluctuation corrections, are determined using different approximations of the chain structure factor for semiflexible polymers. While wormlike-chain statistics provides the most broadly accurate prediction for phase behavior, a Gaussian-rigid interpolation remains an adequate approximation for quadratic-order fluctuation corrections for many experimentally relevant systems. However, our theory provides the basis for predicting the impact of higher-order concentration fluctuations, which requires chain statistics that cannot be rendered from existing approximate methods.

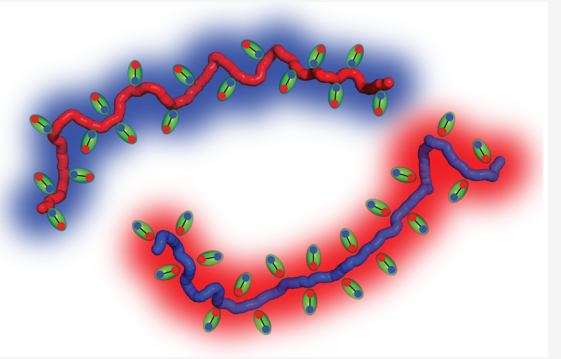

INTRODUCTION

Polyelectrolyte solutions and materials play a central role in a number of applications, ranging from industrial production of food,[1−4] pharmaceuticals,[5−8] adhesives,[9−12] biopolymer phase segregation in living cells,[13−18] and water purification membranes.[19−23] Applications of polyelectrolytes often rely on their tendency to phase separate into a polymer-rich mixture composed of oppositely charged polymers (coacervate) and an ion-rich phase (supernatant) that contains trace amounts of polymers. Progress in our fundamental understanding of complex coacervation has been essential in predicting the thermodynamics[24−28] and morphology[29−31] of both synthetic and naturally occurring polyelectrolytes. However, as discussed in recent reviews,[32−35] there remains a significant challenge in building a theoretical formulation that captures long-range electrostatic correlations and properly relates nanoscale structure and fluctuations to collective thermodynamic behavior.

In addressing these challenges, we develop a theoretical model of a solution of polyelectrolytes within a polar solvent that aims to accurately capture polymer structure and solvent ordering at the nanoscale (see Figure 1). We leverage exact results for the statistical behavior of the wormlike chain model (WLC) in tandem with the random phase approximation (RPA) to accurately incorporate correlated fluctuations across relevant length scales. Our field-theoretic approach incorporates inhomogeneous solvent ordering, resulting in a modified nonlinear Poisson−Boltzmann equation that captures the resulting dielectric inhomogeneity. The combination of solvent ordering and polymer structure facilitates an accurate treatment of electrostatic correlation, which we demonstrate to be critical in predicting thermodynamic behavior.

The theoretical study of polyelectrolyte phase behavior dates back to the Voorn−Overbeak (VO) model,[36,37] which combines a linearized version of the Poisson−Boltzmann equation (i.e., Debye−Hückel theory) with Flory−Huggins polymer-solution theory.[38,39] This model focuses on the complex coacervation of polyanions and polycations in an ionic solution. The use of the linearized Poisson−Boltzmann equation limits the accuracy of the theory to dilute, weakly interacting electrolytes, and the theory disregards polymer chain connectivity, opting to treat the charges along the backbone as disconnected ions. Despite these simplifications, this theory, along with corrective modifications,[40−42] remains a common tool to model experimental data, as its simplicity makes parameter fitting straightforward.

One method to accurately incorporate chain connectivity is the random phase approximation, which extends the mean-

Received: September 2, 2022
Revised: November 29, 2022
Published: December 27, 2022

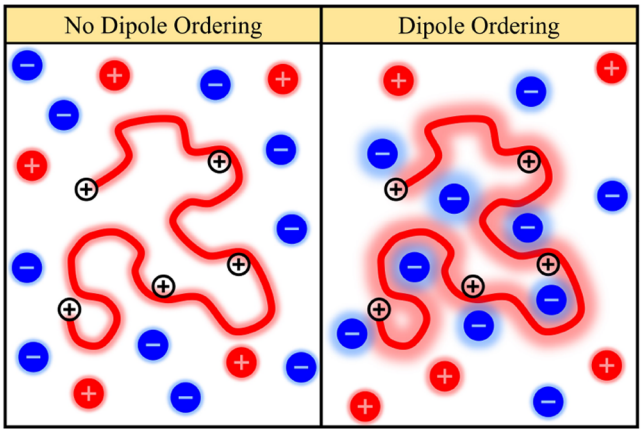

Figure 1. Visualization of the strengths of electrostatic interactions captured within our theory. The left side shows how the treatment of a mixture subject to a consistent dielectric constant experiences equal charge interactions throughout the solution space. On the right, the inclusion of dipole ordering results in an inhomogeneous dielectric constant, leading to more significant charge−charge interactions near the polymers and stronger coupling between polymer and ion concentration fluctuations.

field theory to include concentration fluctuations.[43,44] The success of RPA in uncharged systems, such as block copolymers,[45−47] results in numerous investigations into its use for polyelectrolyte thermodynamics.[48−50] As was expected for charged systems, early literature showed that this formalism was only valid at high polymer density, where concentration fluctuations contribute less significantly to thermodynamic behavior.[48] While RPA is still used in field-theoretic approaches for polyelectrolytes,[51] this approach has limitations in treating charged systems due to the difficult task of capturing accurate correlations from the chain structure, which can lead to unphysical results.[52] Many of these limitations are clearly illustrated in addressing the phase behavior in polyelectrolyte solutions.[53,54] In the case of Coulombic systems, introducing a correction to the mean-field RPA structure factor using a one-loop approximation allows for a more accurate representation of the chain statistics and their impact on collective behavior.[25,55]

RPA theories require an explicit mathematical expression of the chain statistics to describe the spatial distribution of the charged polymer. Commonly, the Gaussian chain structure factor is used to describe flexible chains, but this approach often leads to an overestimation of the correlation effects.[52] Recently, molecular connectivity in charged macromolecules of arbitrary fractal dimensions is explored for fixed structure factors of point-like, rod-like, and coil-like molecules.[56] The statistics of long flexible polymers are well described on length scales comparable to the radius of gyration by the Gaussian chain model,[57] while long stiff polymers can be modeled by the rigid-rod formulation.[58]

The wormlike chain model,[59] which treats the polymer molecules as inextensible elastic chains, is regarded as a comprehensive model that reliably describes the statistical properties ranging from length scales of the entire polymer chain (i.e., the radius of gyration) down to length scales below the polymer persistence length. This multiscale model also includes additional orientational dependence, which becomes important in certain physical systems such as liquid crystals.[60,61] The WLC model, while more accurate, has been historically difficult to incorporate into polymer theory, which has led to its approximation by interpolating between the Gaussian-chain and rigid-rod models.[55] This method can be effective for some solutions, but this approximation fails to accurately model shorter semiflexible polymers where the Gaussian-chain model breaks down.[57] Furthermore, these approximate methods are not currently amenable to theoretical treatments that capture higher-order fluctuation effects (i.e., cubic and quartic), which would serve as the basis for a systematic treatment of solution thermodynamics.

One aspect of charged solutions that requires further investigations is dielectric inhomogeneity associated with solvent-molecule ordering near charged species. While there are numerous investigations into highly correlated charged systems,[62,63] dielectric inhomogeneities present an additional challenge. Commonly, solvent dielectric properties are assumed to be uniform across the polyelectrolyte solution.[37,64] However, nonuniform solvent polarization generated by local electric fields[65,66] is an important contributor to electrostatic correlations.[67−72] For example, dielectric constants are shown to vary from a low value of 5 neighboring the chain to approximately 80 in a bulk aqueous solution (i.e., water as the solvent) over a distance of 2 nm.[73] In the strong coupling limit, the higher multipoles in the ionic network only contribute when there is dielectric inhomogeneity.[74] One method of studying the dielectric response is to explicitly treat the solvent dipole moment within a Poisson−Boltzmann formulation, commonly referred to as the dipolar Poisson−Boltzmann equation (DPBE).[75−79] This approach shows greater electrostatic interactions arising from polarizability, leading to a dielectric gradient between charged species.[80−82]

Further theoretical development is needed to encompass the local polarizability effects in polyelectrolyte solutions, as there are many nontrivial interactions between the charged components such as counterion condensation creating dipoles along the polymer chain[83−86] or charge inversion on surfaces surrounded by multivalent ions.[87−89] Ion pairing on charged polymers results in electrostatic dipoles along the chains[85,86] that can lead to dramatic physical responses such as a coil−globule transition and gel collapse. In polyelectrolyte solutions the importance of including nonuniform dielectric behavior is consistently demonstrated.[90,91] For example, a coarse-grained polarizable particle model is used to investigate the dielectric response of binary mixtures when a uniform electric field is applied,[92] highlighting the coupled structural and electrostatic fluctuations that result from the dielectric properties of the solvent. Some theoretical approaches treat dielectric inhomogeneity by assigning dielectric constants around polymer species,[90,93] with applications that address modifications of the structure of particle suspensions within a charged solution.[94−97]

In our work, we address these challenges by developing a field-theoretic model of polyelectrolyte solutions. The key contribution of this work is the development of an accurate treatment of the semiflexible chain statistics and the incorporation of solvent ordering due to electrostatic correlations. As such, the dielectric inhomogeneity and the solution structure are purely a result of the arrangement of the polar-solvent molecules around the charged species in the mixture. By treating the polymer with the WLC model and accounting for the inhomogeneous dipole ordering, our theory resolves several critical physics effects that are essential in

https://doi.org/10.1021/acs.macromol.2c01826
Macromolecules 2023, 56, 136−152

building a comprehensive theory of polyelectrolyte solution thermodynamics.

We demonstrate the use of this model by addressing two complementary problems. First, we evaluate the electrostatic potential near a charged surface, incorporating dielectric inhomogeneity arising from solvent ordering. This problem provides fundamental insight into the interplay between solvent ordering, electrolyte screening, and electrostatic interaction in a well-defined geometry. Then, we address the phase behavior of a symmetric polyelectrolyte solution, which exhibits inhomogeneous concentration fluctuations whose structure is dictated by the polymer-chain statistics. Therefore, the development of these two problems provides a progressive treatment that captures dielectric inhomogeneity in response to heterogeneous charge distribution and offers a development that facilitates understanding of these physical effects.

THEORETICAL MODEL

We develop a theoretical model of a solution of polyelectrolytes within a polar solvent. Our multicomponent solution includes multiple polymer and ion species to address general thermodynamic phenomena that arise in polyelectrolyte solutions. Once this theory is developed, we turn to specialized systems to illustrate the interplay between the polyelectrolyte solution structure and the inherent environmental polarizability that emerges from the dipole nature of the solvent molecules.

Our mixture contains $n^{(S)}$ solvent molecules. The solvent molecules carry a permanent dipole with charge separation $b^{(S)}$ and charge valency $q^{(S)}$, and each solvent molecule occupies a volume $v^{(S)}$. The instantaneous solvent configuration is defined by the positions $\vec{r}_j^{(S)}$ and orientations $\vec{u}_j^{(S)}$ of the solvent molecules, where $j = 1, 2, ..., n^{(S)}$. The instantaneous solvent volume fraction at position $\vec{r}$ is given by

$$\hat{\phi}^{(S)}(\vec{r}) = v^{(S)} \sum_{j=1}^{n^{(S)}} \delta(\vec{r} - \vec{r}_j^{(S)}) \tag{1}$$

and the instantaneous solvent orientational order parameter is given by

$$\widehat{\vec{D}}^{(S)}(\vec{r}) = v^{(S)} \sum_{j=1}^{n^{(S)}} \vec{u}_j^{(S)} \delta(\vec{r} - \vec{r}_j^{(S)}) \tag{2}$$

where the hatted variables indicate an instantaneous density that depends on the specific configuration of the system. From these definitions, we find the instantaneous solvent charge density to be

$$\begin{aligned} \hat{\rho}^{(S)}(\vec{r}) &= q_s \sum_{j=1}^{n^{(S)}} \left\{ \delta\left[\vec{r} - \left(\vec{r}_j^{(S)} - \frac{b^{(S)}}{2}\vec{u}_j^{(S)}\right)\right] \right. \\ &\quad \left. - \delta\left[\vec{r} - \left(\vec{r}_j^{(S)} + \frac{b^{(S)}}{2}\vec{u}_j^{(S)}\right)\right] \right\} \\ &\approx q^{(S)} b^{(S)} \sum_{j=1}^{n^{(S)}} \vec{u}_j^{(S)} \cdot \vec{\nabla} \delta(\vec{r} - \vec{r}_j^{(S)}) \\ &\approx \frac{q^{(S)} b^{(S)}}{v^{(S)}} \vec{\nabla} \cdot \widehat{\vec{D}}^{(S)} \end{aligned} \tag{3}$$

where the approximate form arises from a small-$b^{(S)}$ expansion and is used throughout this work.

The mixture contains $S^{(I)}$ different ionic species, with the α-species contributing $n^{(I,\alpha)}$ ions to the solution. The α-ion has charge $q^{(I,\alpha)}$ and occupies a molecular volume $v^{(I,\alpha)}$. The instantaneous ion configuration is defined by the position $\vec{r}_j^{(I,\alpha)}$ of the jth ion of the α-species, where $j = 1, 2, ..., n^{(I,\alpha)}$. The instantaneous volume fraction of the α-species is given by

$$\hat{\phi}^{(I,\alpha)}(\vec{r}) = v^{(I,\alpha)} \sum_{j=1}^{n^{(I,\alpha)}} \delta(\vec{r} - \vec{r}_j^{(I,\alpha)}) \tag{4}$$

and the instantaneous ionic charge density is given by

$$\hat{\rho}^{(I)}(\vec{r}) = \sum_{\alpha=1}^{S^{(I)}} q^{(I,\alpha)} \sum_{j=1}^{n^{(I,\alpha)}} \delta(\vec{r} - \vec{r}_j^{(I,\alpha)}) = \sum_{\alpha=1}^{S^{(I)}} \frac{q^{(I,\alpha)}}{v^{(I,\alpha)}} \hat{\phi}^{(I,\alpha)} \tag{5}$$

We combine all ionic species into a single charge density in order to simplify the electrostatic energy terms.

The mixture contains $S^{(P)}$ different polymer species, with the β-species contributing $n^{(P,\beta)}$ polymer chains to the solution. The β-polymer has linear charge density $\lambda^{(P,\beta)}$, chain length $L^{(P,\beta)}$, cross-sectional area $A^{(P,\beta)}$, and persistence length $l_p^{(P,\beta)}$. The linear charge density is smeared evenly along the polymer rather than assigned to individual monomers, which is a good approximation for low electrostatic potential ($|\beta e\psi| \ll 1$).[98] The instantaneous polymer configuration is defined by the space curve $\vec{r}_j^{(P,\beta)}(s^{(P,\beta)})$ of the jth polymer molecule of the β-species, where $j = 1, 2, ..., n^{(P,\beta)}$. The arc-length variable $s^{(P,\beta)}$ gives the position along a chain of the β-species, such that $s^{(P,\beta)} \in [0, L^{(P,\beta)}]$. The instantaneous volume fraction of the β-species is given by

$$\hat{\phi}^{(P,\beta)}(\vec{r}) = A^{(P,\beta)} \sum_{j=1}^{n^{(P,\beta)}} \int_0^{L^{(P,\beta)}} ds^{(P,\beta)} \delta[\vec{r} - \vec{r}_j^{(P,\beta)}(s^{(P,\beta)})] \tag{6}$$

and the instantaneous polymer charge density is given by

$$\begin{aligned} \hat{\rho}^{(P)}(\vec{r}) &= \sum_{\beta=1}^{S^{(P)}} \lambda^{(P,\beta)} \sum_{j=1}^{n^{(P,\beta)}} \int_0^{L^{(P,\beta)}} ds^{(P,\beta)} \delta[\vec{r} - \vec{r}_j^{(P,\beta)}(s^{(P,\beta)})] \\ &= \sum_{\beta=1}^{S^{(P)}} \frac{\lambda^{(P,\beta)}}{A^{(P,\beta)}} \hat{\phi}^{(P,\beta)} \end{aligned} \tag{7}$$

The total charge density in the solution $\hat{\rho}$ is given by the sum of the individual contributions, such that $\hat{\rho} = \hat{\rho}^{(S)} + \hat{\rho}^{(I)} + \hat{\rho}^{(P)}$. Charge neutrality in the solution is enforced by noting that

$$\int d\vec{r} \hat{\rho}(\vec{r}) = \sum_{\alpha=1}^{S^{(I)}} q^{(I,\alpha)} n^{(I,\alpha)} + \sum_{\beta=1}^{S^{(P)}} \lambda^{(P,\beta)} L^{(P,\beta)} n^{(P,\beta)} = 0 \tag{8}$$

We note that the solvent does not contribute to the total charge, since the total charge per solvent molecule is zero. We consider the solution to be incompressible, which is enforced through the constraint

$$\hat{\phi}^{(S)} + \sum_{\alpha=1}^{S^{(I)}} \hat{\phi}^{(I,\alpha)} + \sum_{\beta=1}^{S^{(P)}} \hat{\phi}^{(P,\beta)} = 1 \tag{9}$$

https://doi.org/10.1021/acs.macromol.2c01826
Macromolecules 2023, 56, 136−152

at all positions $\vec{r}$. The polymer chains are modeled using the inextensible wormlike chain model,[59,99] which is enforced by restricting the tangent vectors $\vec{u}_j^{(P,\beta)} = \partial \vec{r}_j^{(P,\beta)}/\partial s^{(P,\beta)}$ to have unit magnitude [i.e., $|\vec{u}_j^{(P,\beta)}(s^{(P,\beta)})| = 1$ for all $s^{(P,\beta)}$, j, and β].

The total energy of the system includes the electrostatic energy, nonelectrostatic two-body interaction energy (i.e., arising from physical interactions excluding those from permanent charge units), and the elastic deformation energy of the polymer chains. In this work, we adopt a simple treatment of the non-electrostatic two-body interactions by assuming Flory−Huggins interaction terms between all of the individual components. Technically, this simplified interaction model is not consistent with the level of treatment of the polymer chains, since semiflexibility would generally lead to orientational contributions. For example, polymer liquid crystallinity is frequently captured at the quadratic order based on a quadrupole-order parameter.[100−102] Such effects can be incorporated into a semiflexible polyelectrolyte model, using our formalism as a foundation.

The system energy for a given configuration is given by

$$\frac{E}{k_BT} = \frac{\epsilon_0}{2k_BT}\int d\vec{r}(\vec{\nabla}\hat{\psi})^2 + \frac{1}{2}\sum_{\gamma_1}\sum_{\gamma_2\neq\gamma_1}\chi_{\gamma_1\gamma_2}\int d\vec{r}\hat{\phi}^{(\gamma_1)}\hat{\phi}^{(\gamma_2)} + \sum_{\beta=1}^{S^{(P)}}\sum_{j=1}^{n^{(P,\beta)}}\frac{l_p^{(P,\beta)}}{2}\int_0^{L^{(P,\beta)}} ds^{(P,\beta)}\left(\frac{\partial \vec{u}_j^{(P,\beta)}}{\partial s^{(P,\beta)}}\right)^2 \tag{10}$$

where k_BT is the thermal energy. The first term represents the electrostatic energy arising from the configuration-dependent electrostatic potential $\hat{\psi}$, which is governed by the Poisson equation $\epsilon_0\nabla^2\hat{\psi} = -\hat{\rho}$. The vacuum permittivity ϵ_0 is used in our treatment since the solvent dipoles are treated explicitly and polarizability naturally emerges based on their correlated fluctuations within the solution. The Flory−Huggins parameter $\chi_{\gamma_1\gamma_2}$ captures the nonelectrostatic two-body interactions between the γ_1-constituent and the γ_2-constituent, where γ is a short-hand index that represents all types of constituents (including solvent, ions, and polymers). Similarly, the volume fraction $\hat{\phi}^{(\gamma)}$ is the instantaneous volume fraction of the γ-constituent. The last term gives the bending deformation energy of the polymer chains based on the wormlike chain model.[59,99]

The thermodynamic behavior of our model is dictated by the canonical partition function

$$Z = \frac{1}{n^{(S)}!(v^{(S)})^{n^{(S)}}}\int\prod_{j^{(S)}=1}^{n^{(S)}} d\vec{r}_{j^{(S)}}^{(S)}d\vec{u}_{j^{(S)}}^{(S)}\prod_{\alpha=1}^{S^{(I)}}\frac{1}{n^{(I,\alpha)}!(v^{(I,\alpha)})^{n^{(I,\alpha)}}} \times\int\prod_{j^{(I,\alpha)}=1}^{n^{(I,\alpha)}} d\vec{r}_{j^{(I,\alpha)}}^{(I,\alpha)}\prod_{\beta=1}^{S^{(P)}}\frac{1}{n^{(P,\beta)}!(A^{(P,\beta)}L^{(P,\beta)})^{n^{(P,\beta)}}} \times\int\prod_{j^{(P,\beta)}=1}^{n^{(P,\beta)}}\mathcal{D}\vec{r}_{j^{(P,\beta)}}^{(P,\beta)}\exp\left(-\frac{E}{k_BT}\right)\prod_{s^{(P,\beta)}}\delta(|\vec{u}_{j^{(P,\beta)}}^{(P,\beta)}(s^{(P,\beta)})| - 1) \prod_{\vec{r}}\delta\left(\hat{\phi}^{(S)} + \sum_{\alpha=1}^{S^{(I)}}\hat{\phi}^{(I,\alpha)} + \sum_{\beta=1}^{S^{(P)}}\hat{\phi}^{(P,\beta)} - 1\right) \tag{11}$$

The inclusion of the molecular volumes in the partition function Z replaces the contribution of the de Broglie wavelengths cubed, which is the standard result from the momentum integrals in the partition function. This replacement merely resets the resulting free energy by a reference free energy.

We now perform a series of field transformations to decouple the interactions, resulting in the partition function being amenable to various levels of approximation. This is done by introducing a series of delta functions that replace the instantaneous volume fractions and charge densities with a fluctuating set of fields. Mathematically, this is accomplished by noting the identity transformation

$$f[\hat{\phi}(\vec{r})] = \int\mathcal{D}\phi\prod_{\vec{r}}\delta[\phi(\vec{r}) - \hat{\phi}(\vec{r})]f[\phi(\vec{r})] = \int\mathcal{D}W_\phi\mathcal{D}\phi\exp\left\{i\int d\vec{r}W_\phi(\vec{r})[\phi(\vec{r}) - \hat{\phi}(\vec{r})]\right\}f[\phi(\vec{r})] \tag{12}$$

which replaces an instantaneous volume fraction $\hat{\phi}$ with a volume fraction field ϕ via a conjugate chemical-potential field W_ϕ. Such a transformation is applied to each of the constituent volume fractions. In addition, the solvent dipole moment $\vec{\hat{D}}^{(S)}$ introduces a solvent dipole field $\vec{D}^{(S)}$ and auxiliary potential field $\vec{W}_D^{(S)}$.

Upon introducing these field variables and performing several transformations, we arrive at the field-transformed partition function

$$Z = \int\mathcal{D}\vec{W}_D^{(S)}\mathcal{D}\vec{D}^{(S)}\prod_\gamma\mathcal{D}W_\phi^{(\gamma)}\mathcal{D}\phi^{(\gamma)} \times\exp\left\{-\frac{\epsilon_0}{2k_BT}\int d\vec{r}(\vec{\nabla}\psi)^2 - \frac{1}{2}\sum_{\gamma_1}\sum_{\gamma_2\neq\gamma_1}\chi_{\gamma_1\gamma_2}\int d\vec{r}\phi^{(\gamma_1)}\phi^{(\gamma_2)} + i\int d\vec{r}\left[\vec{D}^{(S)}\cdot\vec{W}_D^{(S)} + \sum_\gamma W_\phi^{(\gamma)}\phi^{(\gamma)}\right] + \sum_\gamma n^{(\gamma)}\log\left[\frac{z^{(\gamma)}}{v^{(\gamma)}n^{(\gamma)}}\right]\right\}\prod_{\vec{r}}\delta\left(\sum_\gamma\phi^{(\gamma)} - 1\right) \tag{13}$$

where the constituent index γ subsumes all types of molecular constituents. The single-molecule partition function $z^{(\gamma)}$ gives the individual molecular-constituent contribution to the free energy, which depends on the type of constituent. The single-solvent partition function $z^{(S)}$ is given by

$$z^{(S)} = \int d\vec{r}\ d\vec{u}\ \exp[-iv^{(S)}W_\phi^{(S)}(\vec{r}) - iv^{(S)}\vec{u}\cdot\vec{W}_D^{(S)}(\vec{r})] \tag{14}$$

The single-ion partition function $z^{(I,\alpha)}$ is given by

$$z^{(I,\alpha)} = \int d\vec{r}\exp[-iv^{(I,\alpha)}W_\phi^{(I,\alpha)}(\vec{r})] \tag{15}$$

The single-polymer partition function $z^{(P,\beta)}$ is given by

https://doi.org/10.1021/acs.macromol.2c01826
Macromolecules 2023, 56, 136−152

$$z^{(P,\beta)} = \int \mathcal{D}[\vec{r}(s^{(P,\beta)})] \times \exp\left\{ -\frac{l_p^{(P,\beta)}}{2} \int_0^{L^{(P,\beta)}} ds^{(P,\beta)} \left(\frac{\partial \vec{u}}{\partial s^{(P,\beta)}} \right)^2 - iA^{(P,\beta)} \int_0^{L^{(P,\beta)}} ds^{(P,\beta)} W_\phi^{(P,\beta)}(\vec{r}) \right\} \prod_{s^{(P,\beta)}} \delta[|\vec{u}(s^{(P,\beta)})| - 1] \tag{16}$$

At this stage, the partition function Z has not been subjected to any approximations but still is not exactly solvable. However, the field transformations result in a form that is amenable to a number of approximate approaches. In this work, we develop two approaches that permit us to evaluate the thermodynamic behavior of our polyelectrolyte−ion−solvent system. First, we develop a general saddle-point approximation, which determines the thermodynamic state within a mean-field (though potentially inhomogeneous) approximation. Second, we derive the random phase approximation up to quartic order in the volume-fraction fluctuations of the components.

RESULTS AND DISCUSSION

Mean-Field Behavior. We develop the mean-field solution for our system based on a saddle-point approximation. This procedure involves setting the first variation of the integrand of eq 13 to zero, which is consistent with minimizing the system free energy. The field variables $W_\phi^{(\gamma)}$ and $\phi^{(\gamma)}$ are perturbed from a saddle-point value. For example, we set $\phi = \bar{\phi} + \Delta$ in eq 13 (where $\bar{\phi}$ is the saddle-point volume fraction) and expand the integrand up to linear order in Δ (similar for the other field variables).

Upon setting the first variation to zero, we arrive at the saddle-point equations

$$i\bar{W}_\phi^{(S)} = \sum_{\substack{\gamma_2 \neq \gamma_1 \\ \gamma_1 = (S)}} \chi_{\gamma_1\gamma_2} \bar{\phi}^{(\gamma_2)} \tag{17}$$

$$i\vec{\bar{W}}_D^{(S)} = -\frac{q^{(S)} b^{(S)}}{k_B T v^{(S)}} \vec{\nabla}\bar{\psi} \tag{18}$$

$$i\bar{W}_\phi^{(I,\alpha)} = \frac{q^{(I,\alpha)}}{k_B T v^{(I,\alpha)}} \bar{\psi} + \sum_{\substack{\gamma_2 \neq \gamma_1 \\ \gamma_1 = (I,\alpha)}} \chi_{\gamma_1\gamma_2} \bar{\phi}^{(\gamma_2)} \tag{19}$$

$$i\bar{W}_\phi^{(P,\beta)} = \frac{\lambda^{(P,\beta)}}{k_B T A^{(P,\beta)}} \bar{\psi} + \sum_{\substack{\gamma_2 \neq \gamma_1 \\ \gamma_1 = (P,\beta)}} \chi_{\gamma_1\gamma_2} \bar{\phi}^{(\gamma_2)} \tag{20}$$

$$\vec{\bar{D}}^{(S)} = \frac{v^{(S)} n^{(S)}}{\bar{z}^{(S)}} \int d\vec{u}\vec{u} \exp(-iv^{(S)} \bar{W}_\phi^{(S)} - iv^{(S)} \vec{u} \cdot \vec{\bar{W}}_D^{(S)}) \tag{21}$$

$$1 - \sum_{\alpha=1}^{S^{(I)}} \bar{\phi}^{(I,\alpha)} - \sum_{\beta=1}^{S^{(P)}} \bar{\phi}^{(P,\beta)} = \frac{v^{(S)} n^{(S)}}{\bar{z}^{(S)}} \int d\vec{u} \exp(-iv^{(S)} \bar{W}_\phi^{(S)} - iv^{(S)} \vec{u} \cdot \vec{\bar{W}}_D^{(S)}) \tag{22}$$

$$\bar{\phi}^{(I,\alpha)} = \frac{v^{(I,\alpha)} n^{(I,\alpha)}}{\bar{z}^{(I,\alpha)}} \exp(-iv^{(I,\alpha)} \bar{W}_\phi^{(I,\alpha)}) \tag{23}$$

$$\bar{\phi}^{(P,\beta)} = n^{(P,\beta)} A^{(P,\beta)} \int_0^{L^{(P,\beta)}} ds^{(P,\beta)} \langle \delta(\vec{r} - \vec{r}(s^{(P,\beta)})) \rangle_0^{(P,\beta)} \tag{24}$$

The single-chain average $\langle \cdots \rangle_0^{(P,\beta)}$ is defined as a polymer-chain average over the single-chain saddle-point energy

$$\frac{\mathcal{E}_0^{(P,\beta)}}{k_B T} = \frac{l_p^{(P,\beta)}}{2} \int_0^{L^{(P,\beta)}} ds^{(P,\beta)} \left(\frac{\partial \vec{u}(s^{(P,\beta)})}{\partial s^{(P,\beta)}} \right)^2 + iA^{(P,\beta)} \int_0^{L^{(P,\beta)}} ds^{(P,\beta)} \bar{W}_\phi^{(P,\beta)}(\vec{r}) \tag{25}$$

We use the saddle point equation to eliminate $\bar{W}_\phi^{(\gamma)}$ and $\vec{\bar{W}}_D^{(S)}$, resulting in the saddle-point equation governing the electrostatic potential

$$\epsilon_0 \nabla^2 \bar{\psi} = -\frac{q^{(S)} b^{(S)} n^{(S)}}{\bar{z}^{(S)}} \times \int d\vec{u}\vec{u} \cdot \vec{\nabla} \exp\left(-v^{(S)} \sum_{\substack{\gamma_2 \neq \gamma_1 \\ \gamma_1 = (S)}} \chi_{\gamma_1\gamma_2} \bar{\phi}^{(\gamma_2)} + \frac{q^{(S)} b^{(S)}}{k_B T} \vec{u} \cdot \vec{\nabla} \bar{\psi} \right) - \sum_{\alpha=1}^{S^{(I)}} \frac{q^{(I,\alpha)} n^{(I,\alpha)}}{\bar{z}^{(I,\alpha)}} \exp\left(-v^{(I,\alpha)} \sum_{\substack{\gamma_2 \neq \gamma_1 \\ \gamma_1 = (I,\alpha)}} \chi_{\gamma_1\gamma_2} \bar{\phi}^{(\gamma_2)} - \frac{q^{(I,\alpha)}}{k_B T} \bar{\psi} \right) - \sum_{\beta=1}^{S^{(P)}} n^{(P,\beta)} \lambda^{(P,\beta)} \int_0^{L^{(P,\beta)}} ds^{(P,\beta)} \langle \delta(\vec{r} - \vec{r}(s^{(P,\beta)})) \rangle_0^{(P,\beta)} \tag{26}$$

which is a generalized form of the Poisson−Boltzmann equation that includes heterogeneous solvent polarization and constituent demixing due to nonelectrostatic interactions. The three terms on the right-hand side capture inhomogeneous charge density arising from solvent, ions, and polyelectrolyte chains, respectively.

We consider the case $\chi_{\gamma_1\gamma_2} = 0$. We also assume the system exhibits microscopic heterogeneity and bulk homogeneity, which gives $\bar{z}^{(S)} = 4\pi V$ and $\bar{z}^{(I,\alpha)} = V$. This leads to the governing equation

$$\epsilon_0 \nabla^2 \bar{\psi} = -\frac{q^{(S)} b^{(S)} c^{(S)}}{4\pi} \int d\vec{u}\vec{u} \cdot \vec{\nabla} \exp\left(\frac{q^{(S)} b^{(S)}}{k_B T} \vec{u} \cdot \vec{\nabla} \bar{\psi} \right) - \sum_{\alpha=1}^{S^{(I)}} q^{(I,\alpha)} c^{(I,\alpha)} \exp\left(-\frac{q^{(I,\alpha)}}{k_B T} \bar{\psi} \right) - \sum_{\beta=1}^{S^{(P)}} n^{(P,\beta)} \lambda^{(P,\beta)} \int_0^{L^{(P,\beta)}} ds^{(P,\beta)} \langle \delta(\vec{r} - \vec{r}(s^{(P,\beta)})) \rangle_0^{(P,\beta)} \tag{27}$$

which is written entirely in terms of the electrostatic potential $\bar{\psi}$. The first term on the right-hand side represents the

https://doi.org/10.1021/acs.macromol.2c01826
Macromolecules 2023, 56, 136−152

inhomogeneous polarization of the dipole solvent due to local gradients in the electrostatic potential. The remaining terms represent the ion and polymer contributions, respectively. If we assume the gradient in the electrostatic potential is small, this term is approximately written as

$$-\frac{q^{(S)}b^{(S)}c^{(S)}}{4\pi}\int d\vec{u}\vec{u}\cdot\vec{\nabla}\exp\left(\frac{q^{(S)}b^{(S)}}{k_BT}\vec{u}\cdot\vec{\nabla}\overline{\psi}\right) \approx -\frac{(q^{(S)}b^{(S)})^2c^{(S)}}{3k_BT}\nabla^2\overline{\psi} \quad (28)$$

which is equivalent to having an effective dielectric constant $\epsilon = \epsilon_0 + (q^{(S)}b^{(S)})^2c^{(S)}/(3k_BT)$ in our Poisson−Boltzmann equation. However, eq 27 serves as a basis for determining electrostatic potential including spontaneous polarization in response to local electrostatic potential. Ionic volumes are treated only in the incompressibility of the solution, which influences the entropy of mixing, but cannot predict crystallization that would occur due to the electrostatics at high saturation. Furthermore, electrostatic effects that arise from the finite ion size, such as the Born self-energy, are also neglected in our work.

Electrostatic Potential of a Monovalent Salt Solution near a Charged Surface. We evaluate the impact of dipole ordering on the electrostatic potential for the simple case of a charged surface in contact with a monovalent salt solution of concentration $c^{(I)}$ (i.e., equal concentration of positive and negative monovalent ions), which is visualized in Figure 2. The

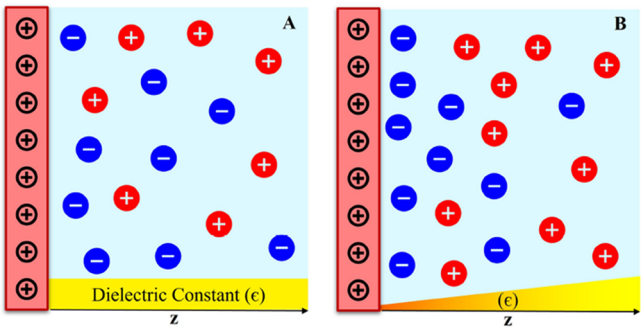

Figure 2. A positively charged surface in a monovalent saltwater solution. The solvent is first treated as a point particle (A) resulting in a constant dielectric medium where charges are evenly shielded throughout the solution space. The solvent is then treated as a dipole (B), which results in an inhomogeneous dielectric constant and greater charge−charge interactions near the surface.

surface has a uniform charge density and is nonpolarizable. The above case removes the polymer term in eq 27, resulting in the solvent-ordered Poisson−Boltzmann equation

$$\epsilon_0\frac{\partial^2\overline{\psi}}{\partial z^2} = 2ec^{(I)}\sinh(e\beta\overline{\psi}) - \frac{q^{(S)}b^{(S)}c^{(S)}}{2}\int_{-1}^{1}d\rho\rho\frac{\partial}{\partial z}\exp\left(\frac{q^{(S)}b^{(S)}}{k_BT}\rho\frac{\partial\overline{\psi}}{\partial z}\right) \quad (29)$$

where we introduce the orientation variable $\rho = \cos\theta = \vec{u}\cdot\hat{\delta}_z$. After a few manipulations found in Appendix A, this equation is converted into a second-order ordinary differential equation (ODE), dependent only in the z direction (normal to the charged surface). We nondimensionalize the equation by setting $\tilde{\psi} = e\beta\overline{\psi}$ and $\eta = z/l_D$, where $l_D = \sqrt{\epsilon/2\beta e^2c^{(I)}}$ is the Debye length of the salt solution for a given concentration of monovalent salt $c^{(I)}$. This substitution leads to the governing equation for the electrostatic potential with inhomogeneous polarization of the dipole solvent, given by

$$\frac{\partial^2\tilde{\psi}}{\partial\eta^2} = \sinh\tilde{\psi} - \tilde{c}\frac{\partial}{\partial\eta}\left[\frac{\tilde{\mu}\frac{\partial\tilde{\psi}}{\partial\eta}\cosh\left(\tilde{\mu}\frac{\partial\tilde{\psi}}{\partial\eta}\right) - \sinh\left(\tilde{\mu}\frac{\partial\tilde{\psi}}{\partial\eta}\right) - \frac{1}{3}\tilde{\mu}^3\left(\frac{\partial\tilde{\psi}}{\partial\eta}\right)^3}{\tilde{\mu}^2\left(\frac{\partial\tilde{\psi}}{\partial\eta}\right)^2}\right] \quad (30)$$

The nondimensionalization of the equation results in an effective solvent concentration $\tilde{c} = l_De^2\beta\mu c^{(S)}/\epsilon$ and effective dipole moment $\tilde{\mu} = q^{(S)}b^{(S)}/(l_De)$, which are defined based on the Debye screening length.

The effective concentration $\tilde{c}$ governs the net impact of solvent ordering on the electrostatic potential. The case $\tilde{c} = 0$ is associated with the absence of a dipole moment μ in the solvent molecules. In this case, the solvent ordering effects are eliminated, and we see the emergence of the nonlinear Poisson−Boltzmann equation

$$\frac{\partial^2\tilde{\psi}}{\partial\eta^2} = \sinh\tilde{\psi} \quad (31)$$

with resulting behavior that is given by the Gouy−Chapman solution.[103,104] We note that nonzero values of $\tilde{c} = l_De^2\beta\mu c^{(S)}/\epsilon$ arise from two competing contributions. The larger dipole content in the solution is governed by $\mu c^{(S)}$, which causes an increase in $\tilde{c}$. However, the degree of electrostatic screening is governed by the factor $\epsilon/(l_De^2\beta)$, which reduces the impact of the electrostatic potential on solvent ordering and reduces the value of $\tilde{c}$. Thus, solvent ordering is enhanced by larger dipole content and in the absence of electrostatic screening under conditions of low salt concentration.

The equation for the electrostatic potential with inhomogeneous polarization of the dipole solvent (eq 30) does not have a readily solvable analytical solution. Instead, we solve it numerically using quartic-order finite differencing along with Newton's method. Defining σ as the surface charge density, we have Neumann boundary conditions with $\frac{\partial\psi}{\partial z}|_{z=0} = -\frac{\sigma}{\epsilon}$ on the edge of the charged surface, and $\psi \to 0$ as $z \to \infty$.

Figure 3 shows the increase in the electrostatic potential of our solvent ordering model (solid) compared to the Gouy−Chapman model (dashed) for a monovalent saltwater solution over varying molarity. We analyze the magnitude of this increase over a range of surface charge densities that represent common membranes for separation processes.[105] While most membranes are negatively charged, we have chosen to analyze a positive surface to match the electrostatic potential diagrams to what is more commonly presented. We see a substantial increase in the electrostatic potential on length scales comparable to the Debye length. For a surface charge density of 0.30 C/m^2 there is nearly a 35% increase in the electrostatic potential over the entire distance normal to the surface. We can expand this analysis to a general solution for the increase in electrostatic potential at the boundary of the charged surface and salt solution over a range of different salt solutions and membrane concentrations.

https://doi.org/10.1021/acs.macromol.2c01826
Macromolecules 2023, 56, 136−152

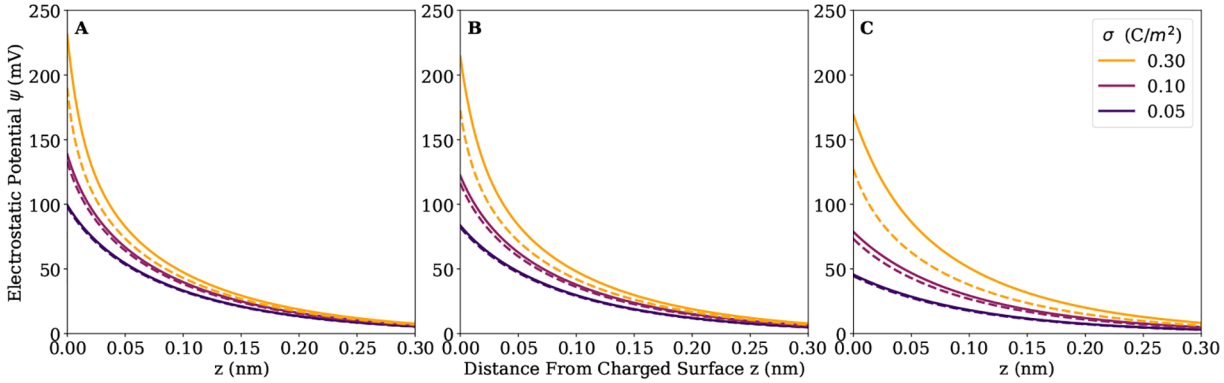

Figure 3. Increase in electrostatic potential compared to the Gouy−Chapman diffuse model (dashed) to our solvent ordering model (solid) for different salt concentrations (A) 0.006 M, (B) 0.06 M, and (C) 0.6 M and over a range of surface charge densities σ = 0.05 C/m^2, 0.10 C/m^2, and 0.30 C/m^2. In the diffuse model, there is a constant dielectric medium resulting in equal electrostatic shielding throughout the solution space. Within our model, the solvent ordering results in an uneven dielectric medium and greater electrostatic interactions near the charged surface.

Figure 4 shows that at high membrane charge densities, the relationship to the percent increase in electrostatic potential is

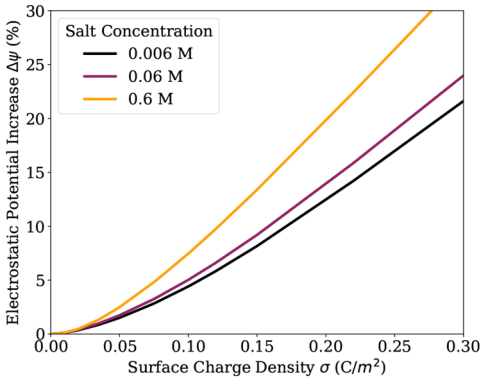

Figure 4. Percent increase in electrostatic potential from the Gouy−Chapman model to our solvent ordering model as a function of surface charge density at z = 0 for different salt concentrations.

roughly linear. Similarly, as the salt concentration increases, we see that the effect of dipole reordering on the electrostatic potential is greater. This trend does not continue indefinitely, and there is a sharp decline in the difference in electrostatic potential for nonphysical salt concentrations that exceed the solubility limit of the solution. Additionally, our theory is not meant to handle these high salt concentrations and would need modifications before any conclusions can be drawn about the solution properties.

Physically, an ionic solution with a polar solvent experiences the local ordering of the solvent around the charged species. This process shields the electrostatic effects of the ions and increases the dielectric constant ϵ of the medium. When we introduce a charged surface near these molecules, we have now imposed a new force on the solvent dipoles that can reorder them away from the charged species and more in line with the electric fields generated by the charged surface. This decreases the ability of the solvent to shield the electrostatic interactions. The effect is a local decrease of the dielectric constant and an effective increase in the electrostatic potential. Dielectric inhomogeneities around charged species also affect the ions' Born solvation energies, which result in unequal ion partitioning[91,106−108] into the higher dielectric region. These effects often merit an explicit treatment which can be included through a Born self-energy augmented Poisson−Boltzmann theory.[109] Our current study does not address Born self-energy arising from finite ion size, and future theoretical work is needed to combine solvent ordering with ion solvation energy.

Fluctuations. We now specialize our theory to the homogeneous phase and subsequently develop the fluctuation free energy in this section. The saddle-point free energy βF_0 is based on the homogeneous-phase saddle-point equations, resulting in the expression

$$\frac{\beta F_0}{V} = \frac{\overline{\phi}^{(S)}}{\nu^{(S)}}\log \overline{\phi}^{(S)} + \sum_{\alpha} \frac{\overline{\phi}^{(I,\alpha)}}{\nu^{(I,\alpha)}}\log \overline{\phi}^{(I,\alpha)} + \sum_{\beta} \frac{\overline{\phi}^{(P,\beta)}}{L^{(P,\beta)}A^{(P,\beta)}}\log \overline{\phi}^{(P,\beta)} + \frac{1}{2}\sum_{\gamma_1,\gamma_2} \chi_{\gamma_1\gamma_2}\overline{\phi}^{(\gamma_1)}\overline{\phi}^{(\gamma_2)} \tag{32}$$

We note that charge neutrality ensures that electrostatic interactions do not contribute to the homogeneous saddle-point free energy.

We now develop the solution for the thermodynamic behavior based on a random-phase approximation up to quartic order in volume-fraction fluctuations. Given the number of components in our theory, we need to adopt a compact notation for summing over the degrees of freedom. Our previous work on random copolymers serves as a basis for establishing a compact framework for summing over components in our system.[110]

Our system has a total number of species $S = 1 + S^{(I)} + S^{(P)}$. We define the vector of auxiliary variables $W = [\{W_\phi\}, \vec{W}_D^{(S)}]$, which contains $S + 3$ terms, one for each species and 3 for the dipole conjugate $\vec{W}_D^{(S)}$. We expand about the homogeneous phase with volume fractions $\overline{\phi}^{(\gamma)}$, such that $\phi^{(\gamma)} = \overline{\phi}^{(\gamma)} + \Delta^{(\gamma)}$ from each of the S species. We then define the concentration fluctuation vector $\Delta = [\{\Delta^{(I,\alpha)}\},\{\Delta^{(P,\beta)}\},\vec{D}]$ (total of $S - 1 + 3$ terms), and we note that $\Delta^{(S)} = -\sum_\alpha \Delta^{(I,\alpha)} - \sum_\beta \Delta^{(P,\beta)}$ ensures the incompressibility constraint is satisfied.

With these definitions, we expand the free energy within eq 13 as

$$-\beta F = -\beta F_0 - \frac{1}{2}V_{\bar{1}\bar{2}}\Delta_{\bar{1}}\Delta_{\bar{2}} + i\Delta_{\bar{1}}W_{\bar{1}} - \frac{1}{2}G^{(2)}_{\bar{1}\bar{2}}W_{\bar{1}}W_{\bar{2}} + \frac{i}{3!}G^{(3)}_{\bar{1}\bar{2}\bar{3}}W_{\bar{1}}W_{\bar{2}}W_{\bar{3}} + \frac{1}{4!}G^{(4)}_{\bar{1}\bar{2}\bar{3}\bar{4}}W_{\bar{1}}W_{\bar{2}}W_{\bar{3}}W_{\bar{4}} \tag{33}$$

https://doi.org/10.1021/acs.macromol.2c01826
Macromolecules 2023, 56, 136−152

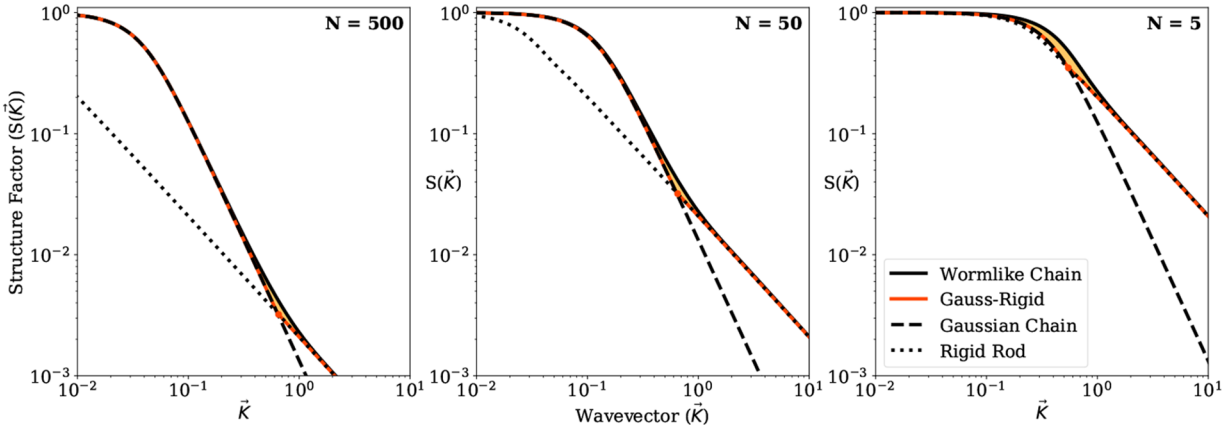

Figure 5. Structure factors of a rigid rod, Gaussian chain, and the exact solution of a wormlike chain versus $\vec{K} = 2l_p\vec{k}$ for different degrees of polymerization (A) $N = 500$, (B) $N = 50$, and (C) $N = 5$, where the monomer length and persistence length are equivalent. The wormlike chain model is approximated by the Gauss-rigid model which crosses over from the Gaussian chain to the rigid rod formulations. The orange area in the plots represents the deviation of the Gauss-rigid model from the more statistically accurate wormlike chain.

Here, we adopt an extended Einstein notation to reduce the summations and integrations involved in the terms within the RPA. The numbered and barred subscripts indicate summation over the $S + 3$ constituents and integration over the Fourier variable $\vec{k}$ (transformed from spatial position $\vec{r}$). For example, the term $G^{(2)}_{\bar{1}\bar{2}}W_{\bar{1}}W_{\bar{2}}$ is written in expanded form as

$$G^{(2)}_{\bar{1}\bar{2}}W_{\bar{1}}W_{\bar{2}} = \frac{1}{(2\pi)^6}\sum_{\gamma_1,\gamma_2}\int d\vec{k}_1 d\vec{k}_2 G^{(2)}_{\gamma_1\gamma_2}(\vec{k}_1,\vec{k}_2)W^{(\gamma_1)}(\vec{k}_1)W^{(\gamma_2)}(\vec{k}_2) \tag{34}$$

The interaction potential $V_{\bar{1}\bar{2}}$ is given by

$$V_{\bar{1}\bar{2}} = \chi_{\gamma_1\gamma_2} + Q_{\gamma_1}Q_{\gamma_2}\frac{1}{k_BT\epsilon_0}\frac{1}{k^2} \tag{35}$$

which accounts for the Flory−Huggins mixing enthalpy and electrostatic interactions resulting from volume-fraction fluctuations (note, $\chi_{\gamma_1\gamma_1} = 0$). We define a constituent charge density Q_γ to define how each constituent contributes to the charge density, such that $Q_{(I,\alpha)} = q^{(I,\alpha)}/v^{(I,\alpha)}$, $Q_{(P,\beta)} = \lambda^{(P,\beta)}/A^{(P,\beta)}$, $Q_S = 0$, and $Q_D = -ikq^{(S)}b^{(S)}/v^{(S)}$.

The terms $G^{(n)}$ arise from the W-field expansion of the single-molecular partition functions. Thus, these terms represent the single-molecule contributions to the local structural organization within the fluid. There exist three types of structure factors associated with solvent, ion, and polymer. In our current theory, the molecular contributions are decoupled such that there are no intermolecular couplings. Within the solvent expansion, there are cross terms between $W^{(S)}_\phi$ and $\vec{W}^{(S)}_D$ that depend on the order n of the expansion.

The solvent single-molecule partition function results in the expansion terms

$$G^{(n)}_{\gamma_1\cdots\gamma_n} = \bar{\phi}^{(S)}(v^{(S)})^{n-1}(2\pi)^3\delta\left(\sum_{i=1}^{n}\vec{k}_i\right)M^{(n)}_{\gamma_1\cdots\gamma_n} \tag{36}$$

for the instances where the species indices γ are given by solvent S (i.e., coupling to $W^{(S)}_\phi$) or $\vec{D}$ (i.e., coupling to $\vec{W}^{(S)}_D$). The solvent coupling matrix $M^{(n)}_{\gamma_1\cdots\gamma_n}$ gives the coupling between $W^{(S)}_\phi$ and $\vec{W}^{(S)}_D$ within the expansion terms. The coupling matrix is provided in Appendix B. The delta-function constraint on the wavevectors $\{\vec{k}\}$ arises from translational invariance of the structure within the homogeneous saddle point. The α-species of ion results in an expansion term of the form

$$G^{(n)}_{\gamma_1\cdots\gamma_n} = \bar{\phi}^{(I,\alpha)}(v^{(I,\alpha)})^{n-1}(2\pi)^3\delta\left(\sum_{i=1}^{n}\vec{k}_i\right) \tag{37}$$

for the instances where all of the species indices γ are given by (I, α).

The β-species of polymer contributes an expansion term

$$G^{(n)}_{\gamma_1\cdots\gamma_n} = \bar{\phi}^{(P,\beta)}(A^{(P,\beta)}L^{(P,\beta)})^{n-1} \times (2\pi)^3\delta\left(\sum_{i=1}^{n}\vec{k}_i\right)S^{(n,P,\beta)}(\{\vec{k}\}) \tag{38}$$

for the instances where all of the species indices γ are given by (P, β). We define the n-point structure factor of the β-species of polymer to be

$$S^{(n,P,\beta)}(\{\vec{k}\}) = \frac{1}{(L^{P,\beta})^n}\prod_{j=1}^{n}\left(\int_0^{L^{(P,\beta)}} ds_j\right) \times \langle\exp[-i\vec{k}_1\cdot\vec{r}^{(P,\beta)}(s_1)]\ldots\exp[-i\vec{k}_n\cdot\vec{r}^{(P,\beta)}(s_n)]\rangle_0 \tag{39}$$

The angle brackets $\langle\cdots\rangle_0$ indicate a single-chain thermodynamic average (i.e., with respect to $\beta\mathcal{E}^{(1,P,\beta)}_0$ from eq 25 with $\bar{W}^{(P,\beta)}_\phi = 0$). The polymer structure factor defines the chain connectivity contribution to the fluid structure. The wormlike chain structure factor is expressed

$$S^{(2)}_{WC}(k) = \frac{2}{N^2}\mathcal{L}^{-1}_{p\to N}\left\{\frac{\tilde{G}(K;p)}{p^2}\right\} \tag{40}$$

with

$$\tilde{G}(K;p) = \frac{1}{P_0 + \frac{a_1^2K^2}{P_1 + \frac{a_2^2K^2}{P_{2+\ldots}}}} \tag{41}$$

where $N = L/(2l_p)$ and $K = 2l_p|\vec{k}|$. We note $\mathcal{L}^{-1}$ indicates Laplace inversion from p to N. A more detailed calculation of the wormlike chain structure factor is described in previous work.[111−114]

https://doi.org/10.1021/acs.macromol.2c01826
Macromolecules 2023, 56, 136−152

Due to the complexity of solving eq 39, which gives the exact solution to the wormlike chain, the polymer structure factors are often approximated with simpler models. The Gaussian chain model is the well-known Debye function[115]

$$S^{(2)}_{GC}(k) = \frac{2}{k^4 R_g^4}[\exp(-k^2R_g^2) - 1 + k^2R_g^2] \tag{42}$$

which is accurate for long flexible polymers that follow Gaussian chain statistics.

The radius of gyration is calculated $R_g = \sqrt{b^2N/6}$. The Kuhn statistical segment length b is twice the persistence length l_p of the polymer. The other relevant structure factor definition is that of a rigid rod.[58] It is accurate in high k for short stiff polymers and is defined as

$$S^{(2)}_{RR}(k) = \frac{2}{kL}\mathrm{Si}(kL) - \frac{4}{(\mathrm{kL})^2}\sin^2\left(\frac{kL}{2}\right) \tag{43}$$

where $\mathrm{Si}(x) = \int_0^x dy(\sin y)/y$ is the Sin integral $\mathrm{Si}(x)$. These two structure factors define the limits of very flexible (eq 42) and fully rigid (eq 43) polymers. Figure 5 plots the structure factor for semiflexible polymers with a persistence and monomer length of 3 nm for different lengths of polymers. One method of approximating the wormlike chain model is to interpolate between the Gaussian chain and the rigid rod formulations or crossover at the point where they intersect. This approach has been labeled as the Gauss-rigid model, as it is a combination of both limiting behaviors. For long polymers that are more flexible, this approximation is quite accurate, as shown in the leftmost plot of Figure 5 with a degree of polymerization of 500. However, for short, semiflexible polymers both the Gaussian chain and rigid rod fail to accurately represent the true chain statistics. This can be best visualized for $N = 5$, where the semiflexibility of the short polymer causes both the Gaussian chain model and rigid rod to severely underpredict the structure factor.

We eliminate W from the free energy by finding the maximum value in the functional integration. This results in the free energy

$$-\beta F = -\beta F_0 - \frac{1}{2}\Gamma^{(2)}_{\bar{1}\bar{2}}\Delta_{\bar{1}}\Delta_{\bar{2}} + \frac{1}{3!}\Gamma^{(3)}_{\bar{1}\bar{2}\bar{3}}\Delta_{\bar{1}}\Delta_{\bar{2}}\Delta_{\bar{3}} + \frac{1}{4!}\Gamma^{(4)}_{\bar{1}\bar{2}\bar{3}\bar{4}}\Delta_{\bar{1}}\Delta_{\bar{2}}\Delta_{\bar{3}}\Delta_{\bar{4}} \tag{44}$$

The resulting vertex functions are written as

$$\Gamma^{(2)}_{\bar{1}\bar{2}} = \chi_{\gamma_1\gamma_2}(2\pi)^3\delta(\vec{k}_1 + \vec{k}_2) + Q_{\gamma_1}Q_{\gamma_2}\frac{1}{k_BT\epsilon_0}\frac{1}{k^2}(2\pi)^3\delta(\vec{k}_1 + \vec{k}_2) + G^{(2)^{-1}}_{\bar{1}\bar{2}} \tag{45}$$

$$\Gamma^{(3)}_{\bar{1}\bar{2}\bar{3}} = G^{(3)}_{\bar{1}'\bar{2}'\bar{3}'}G^{(2)^{-1}}_{\bar{1}'\bar{1}}G^{(2)^{-1}}_{\bar{2}'\bar{2}}G^{(2)^{-1}}_{\bar{3}'\bar{3}} \tag{46}$$

$$\Gamma^{(4)}_{\bar{1}\bar{2}\bar{3}\bar{4}} = G^{(4)}_{\bar{1}'\bar{2}'\bar{3}'\bar{4}'}G^{(2)^{-1}}_{\bar{1}'\bar{1}}G^{(2)^{-1}}_{\bar{2}'\bar{2}}G^{(2)^{-1}}_{\bar{3}'\bar{3}}G^{(2)^{-1}}_{\bar{4}'\bar{4}} - 3G^{(3)}_{\bar{1}'\bar{2}'\bar{5}}G^{(3)}_{\bar{3}'\bar{4}'\bar{6}}G^{(2)^{-1}}_{\bar{5}\bar{6}}G^{(2)^{-1}}_{\bar{1}'\bar{1}}G^{(2)^{-1}}_{\bar{2}'\bar{2}}G^{(2)^{-1}}_{\bar{3}'\bar{3}}G^{(2)^{-1}}_{\bar{4}'\bar{4}} \tag{47}$$

The incompressibility constraint requires that the sum of the volume-fraction fluctuations is zero, i.e., $\sum_{\gamma=1}^{S}\Delta^{(\gamma)} = 0$. Thus, we can eliminate one of the components from the treatment, and we choose to eliminate the solvent volume-fraction fluctuations by setting $\Delta^{(S)} = -\sum_{\gamma\neq S}\Delta^{(\gamma)}$. The solvent dipole moment $\vec{D}$ remains in the treatment and includes coupling to volume-fraction fields. However, this coupling only exists at cubic and quartic (and higher order). We eliminate $\vec{D}$ from the RPA by determining the maximum value in the functional integral with respect to fluctuations in $\vec{D}$.

This now leads to a free-energy expansion in terms of the volume fraction fluctuations of the ion and polymer constituents. The free energy is now written in the form

$$-\beta F = -\beta F_0 - \frac{1}{2}\Gamma^{(2,\phi)}_{\tilde{1}\tilde{2}}\Delta_{\tilde{1}}\Delta_{\tilde{2}} + \frac{1}{3!}\Gamma^{(3,\phi)}_{\tilde{1}\tilde{2}\tilde{3}}\Delta_{\tilde{1}}\Delta_{\tilde{2}}\Delta_{\tilde{3}} + \frac{1}{4!}\Gamma^{(4,\phi)}_{\tilde{1}\tilde{2}\tilde{3}\tilde{4}}\Delta_{\tilde{1}}\Delta_{\tilde{2}}\Delta_{\tilde{3}}\Delta_{\tilde{4}} \tag{48}$$

We have modified the extended Einstein notation such that the subscripts with a tilde now indicate summation only over the volume-fraction fluctuations of the ion and polymer constituent volume fractions (i.e., summation over $S^{(I)}$ ion species and $S^{(P)}$ polymer species) and integration over the Fourier variables. The volume-fraction vertex functions $\Gamma^{(n,\phi)}_{\tilde{1}\cdots\tilde{n}}$ represent the contributions to the free energy from volume-fraction fluctuations, here captured up to quartic order.

The quadratic-order theory is governed by the vertex function

$$\Gamma^{(2,\phi)}_{\tilde{1}\tilde{2}} = \chi_{\gamma_1\gamma_2}(2\pi)^3\delta(\vec{k}_1 + \vec{k}_2) + Q_{\gamma_1}Q_{\gamma_2}\frac{1}{k_BT\epsilon}\frac{1}{k_1^2}(2\pi)^3\delta(\vec{k}_1 + \vec{k}_2) + G^{(2)^{-1}}_{\tilde{1}\tilde{2}} \tag{49}$$

where $\epsilon = \epsilon_0 + (\mathrm{q}^{(S)}b^{(S)})^2c^{(S)}/3k_BT$. The free energy within the quadratic-order RPA after integration over density fluctuations is then given by

$$\beta F = \beta F_0 + \frac{1}{2}\frac{V}{(2\pi)^3}\sum_{\gamma=1}^{S^{(I)}+S^{(P)}}\int d\vec{k}\log\lambda_\gamma \tag{50}$$

where λ_γ represents the set of eigenvalues of the $\mathbf{\Gamma}^{(2,\phi)}$ matrix. This matrix has elements for all of the $S^{(I)} + S^{(P)}$ constituents, resulting in a summation over γ from 1 to $S^{(I)} + S^{(P)}$. We introduce a reference state of a noninteracting solution where Flory–Huggins and electrostatic interactions are switched off, $\chi_{\gamma_1\gamma_2} = Q_{\gamma_1} = 0$. This results in a noninteracting vertex-function matrix, written as $\mathbf{\Gamma}^{(2,\phi)}_0$ with eigenvalues $\lambda^{(0)}_\gamma$. The resulting reference free energy is given by

$$\beta F_{\mathrm{ref}} = \frac{1}{2}\frac{V}{(2\pi)^3}\sum_{\gamma=1}^{S^{(I)}+S^{(P)}}\int d\vec{k}\,\log\lambda^{(0)}_\gamma \tag{51}$$

By subtracting off this noninteracting reference state, we redefine βF with a reference free energy. Noting the spherical symmetry in the quadratic-order contribution, we obtain

$$\beta F = \beta F_0 + \frac{V}{4\pi^2}\sum_{\gamma=1}^{S^{(I)}+S^{(P)}}\int_0^\Lambda dk k^2\log\lambda_\gamma - \frac{V}{4\pi^2}\sum_{\gamma=1}^{S^{(I)}+S^{(P)}}\int_0^\Lambda dk k^2\log\lambda^{(0)}_\gamma \tag{52}$$

We also introduce a k-cutoff at Λ to account for the ultraviolet divergence in the high-k limit. The k-cutoff is chosen to be on the length scale of the smallest persistence length of the polymer components, such that $\Lambda = 2\pi/l_p^{(P,\beta)}$. For $k > \Lambda$ (i.e., length scale below $1/\Lambda$), the k-contribution to the free energy

https://doi.org/10.1021/acs.macromol.2c01826
Macromolecules 2023, 56, 136−152

is neglected due to the theory being unable to capture physical behavior below this length scale.

The free energy equation can be additionally reduced by utilizing the eigenvalue property $\prod_\gamma \lambda_\gamma = |\mathbf{\Gamma}^{(2,\phi)}|$, i.e., the product of all the eigenvalues of a matrix is equal to the determinant of the associated matrix. The sum over the logs of all the eigenvalues can now be reduced to the log of the determinant. The free energy up to quadratic order is now expressed as

$$\beta F = \beta F_0 + \frac{V}{4\pi^2}\int_0^\Lambda dk k^2 \log\left(\frac{|\mathbf{\Gamma}^{(2,\phi)}|}{|\mathbf{\Gamma}_0^{(2,\phi)}|}\right) \tag{53}$$

which serves as the basis for thermodynamic analyses using the quadratic-order RPA.

Phase Phenomena. Theory validation is frequently approached by calculating the theoretical phase behavior and comparing the results to highly validated models and/or experimental work. There are many investigations on experimental phase behavior.[116−125] Systematic exploration of polyelectrolyte phase behavior is challenging due to the many variables involved in the observed behavior. These variables include polymer length and stiffness, charge distribution along the backbone, ion size and valency, and dielectric inhomogeneities. Most approaches focus on phase behavior as a function of salt concentration. For a single polyelectrolyte species (with counterions) in a salt solution, the solution is stable until a critical salt concentration is met and phase separation occurs. This minimum salt concentration is an effect of reducing the entropic cost of phase separating the polymer and salt species. As more salt is added, the solution becomes stable again, which creates a loop in the phase diagram. At this higher salt concentration, the ions screen the electrostatic interactions, and the two phases become more compatible, ultimately leading to one homogeneous phase. In symmetric blends with two oppositely charged polymers, this loop does not exist for low salt concentrations, as it is entropically favorable for the charged polymers to associatively phase separate and release the counterions.

Our polymer field-theoretic model enables a prediction of the phase behavior of a polyelectrolyte solutions based on the quadratic-order RPA developed in the preceding subsections. The phase diagram for a polyelectrolyte solution is determined by equating the chemical potentials between the two phases for each of the species. Using eq 53, we derive the generalized quadratic-order chemical potential. We break these calculations into the homogeneous chemical potential $\mu_0^{(\gamma)}$ and quadratic-order chemical potential $\mu_2^{(\gamma)}$ for γ-species in the polyelectrolyte solution. The general form of the chemical potential equation is calculated by differentiation of the Helmholtz free energy with respect to the mole number $n^{(\gamma)}$ of the γ-species in the solution. Due to the incompressibility constraint, we note that the Helmholtz free energy is equivalent to the Gibbs free energy. We define γ-species chemical potential as

$$\mu^{(\gamma)} = \frac{\partial F}{\partial n^{(\gamma)}} \tag{54}$$

We also introduce an intensive free energy $f = F/V$, which captures the sum of the mean-field intensive free energy f_0 and quadratic-order intensive free energy f_2. Noting that volume is a function of $n^{(\gamma)}$ such that $V = \sum_{\gamma=1}^{S} n^{(\gamma)} v^{(\gamma)}$, we write the general expression for the chemical potential as

$$\begin{aligned}\beta\mu^{(\gamma)} &= \frac{\partial}{\partial n^{(\gamma)}}(V\beta f)\\ &= \beta f v^{(\gamma)} + V\frac{\partial \beta f}{\partial n^{(\gamma)}}\end{aligned} \tag{55}$$

The mean-field chemical potential for the γ-component is written as

$$\begin{aligned}\beta\mu_0^{(\gamma)} = \log\bar{\phi}^{(\gamma)} + 1 - \sum_{\gamma_1}\frac{v^{(\gamma)}}{v^{(\gamma_1)}}\bar{\phi}^{(\gamma_1)}\\ - \frac{v^{(\gamma)}}{2}\sum_{\gamma_1\gamma_2}\chi_{\gamma_1\gamma_2}\bar{\phi}^{(\gamma_1)}\bar{\phi}^{(\gamma_2)} + v^{(\gamma)}\sum_{\gamma_1}\chi_{\gamma\gamma_1}\bar{\phi}^{(\gamma_1)}\end{aligned} \tag{56}$$

The quadratic-order chemical potential is calculated similarly by taking the derivative of the quadratic-order free energy term f_2, which is the second term on the RHS of eq 53. This results in the generalized expression

$$\begin{aligned}\beta\mu_2^{(\gamma)} = \beta f_2 v^{(\gamma)} + \frac{V}{4\pi^2}\int_0^\Lambda dk \sum_{\gamma_1}\frac{k^2}{|\mathbf{\Gamma}^{(2,\phi)}|}\frac{\partial|\mathbf{\Gamma}^{(2,\phi)}|}{\partial\phi^{(\gamma_1)}}\frac{\partial\phi^{(\gamma_1)}}{\partial n^{(\gamma)}}\\ - \frac{V}{4\pi^2}\int_0^\Lambda dk \sum_{\gamma_1}\frac{k^2}{|\mathbf{\Gamma}_0^{(2,\phi)}|}\frac{\partial|\mathbf{\Gamma}_0^{(2,\phi)}|}{\partial\phi^{(\gamma_1)}}\frac{\partial\phi^{(\gamma_1)}}{\partial n^{(\gamma)}}\end{aligned} \tag{57}$$

This form of the quadratic-order chemical potential allows us to utilize Jacobi's formula to calculate the derivative of the determinant for an invertible matrix $\boldsymbol{A}(x)$ over its determinant, given by

$$\frac{1}{|\boldsymbol{A}|}\frac{\partial|\boldsymbol{A}|}{\partial x} = \mathrm{Tr}\left(\boldsymbol{A}^{-1}\cdot\frac{\partial\boldsymbol{A}}{\partial x}\right) \tag{58}$$

In this expression, $\partial\boldsymbol{A}/\partial x$ is an element-wise derivative of $\boldsymbol{A}$ with respect to x and $\boldsymbol{A}^{-1}$ is the inverse matrix of $\boldsymbol{A}$. The total chemical potential for an individual species is the sum of the mean-field and quadratic-order chemical potential written as $\beta\mu^{(\gamma)} = \beta\mu_0^{(\gamma)} + \beta\mu_2^{(\gamma)}$. Up to this point, we have developed all of the equations we need to determine the phase behavior of polyelectrolyte solutions of arbitrary size.

The spinodal of a polyelectrolyte solution marks the limit of stability of the homogeneous phase. This is calculated by identification of conditions where $|\mathbf{\Gamma}^{(2,\phi)}(\vec{k}^*)| = 0$. We define $\vec{k}^*$ as the critical wavevector associated with the largest fluctuation. The magnitude of fluctuations scales with the inverse of the eigenvalues of the $\mathbf{\Gamma}^{(2,\phi)}$ matrix; thus as an eigenvalue goes to zero, the fluctuations become infinitely unstable.

To calculate the binodal curve, we first determine the critical point through a search along the spinodal curve. This is the point at which the binodal and spinodal curves intersect and is the ideal spot to begin our iterative algorithm for determining the entire binodal curve. This location is found where the dominant solution fluctuations are parallel to the spinodal curve. At the critical point, the fluctuation direction tells us the concentration shifts that the two phases will follow. Thus, when the binodal and spinodal intersect, the dominant fluctuation must be along the curves. By contracting the third-order vertex function with the dominant eigenvectors $\vec{\varepsilon}$

https://doi.org/10.1021/acs.macromol.2c01826
Macromolecules 2023, 56, 136−152

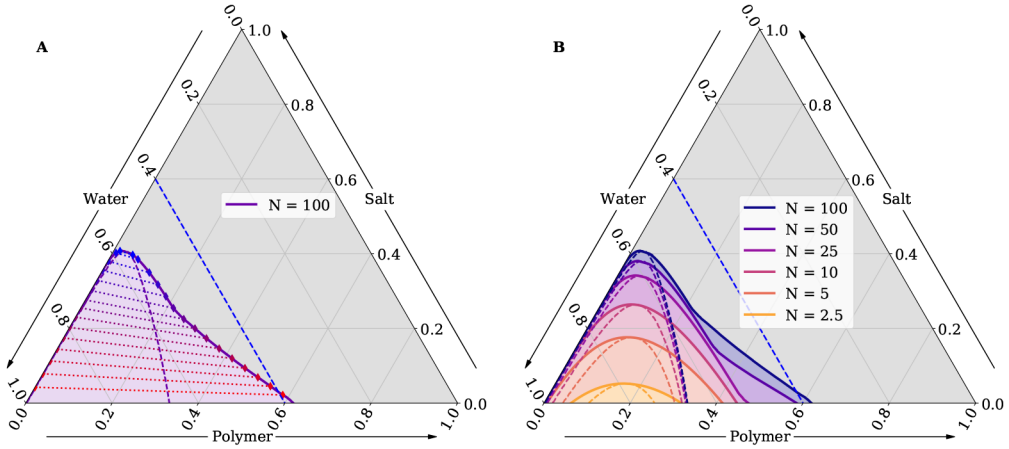

Figure 6. (A) Mean-field binodal (solid) and spinodal curves (dashed) plotted on a ternary phase diagram for a symmetric polyelectrolyte solution with chain length $N = 100$ for the polycation and polyanion. The mean-field binodal is only influenced by Flory–Huggins interactions and is unable to capture electrostatic contributions to the free energy. Tie-lines (dotted) are included to show the direction in which phase separation occurs and the compositions of the two phases in coexistence. (B) Mean-field binodal and spinodal diagrams with $N = 2.5$, 5, 10, 25, 50, and 100 are shown to illustrate the effect of increasing chain length on phase separation. Both plots contain a dashed blue line to indicate the region of interest that is analyzed in the quadratic-order binodal plots.

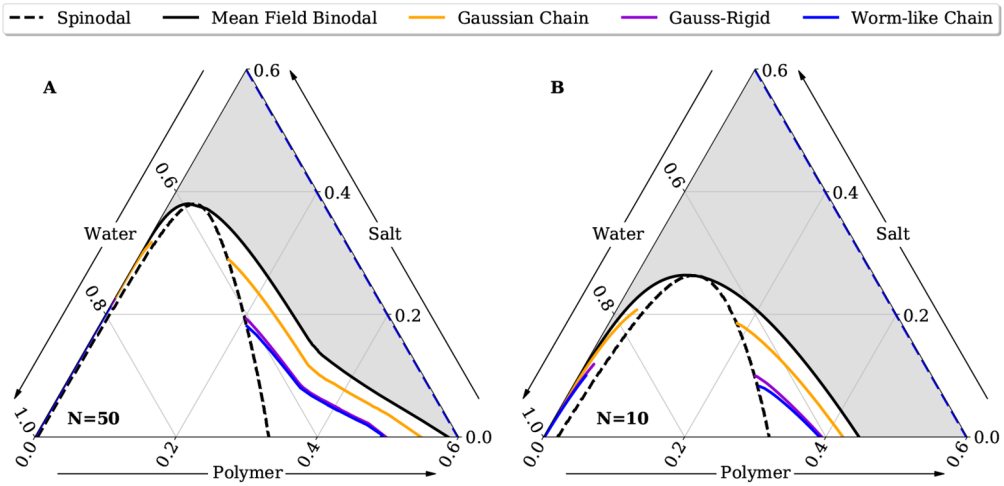

Figure 7. Quadratic-order binodal curves for a symmetric polyelectrolyte solution for $N = 50$ (A) and $N = 10$ (B). For each polymer length, the solution is plotted for different structure factor definitions. The Gaussian chain model (orange), most accurate for flexible polymers, is contrasted against the wormlike chain model (blue), which captures the correct statistics at all length scales, and the Gauss-rigid model (purple), which closely approximates the WLC model. The quadratic-order binodals are plotted outside of the spinodal region where the fluctuations cannot be incorporated into the free energy and against the mean-field binodal to demonstrate the effect of including concentration fluctuations within the model.

for each point on the spinodal, we identify critical points by finding the solution to

$$\Gamma^{(3,\phi)}_{\tilde{1}\tilde{2}\tilde{3}}(k_{\tilde{1}}, k_{\tilde{2}}, k_{\tilde{3}})\vec{\varepsilon}_{\tilde{1}}(k^*)\vec{\varepsilon}_{\tilde{2}}(k^*)\vec{\varepsilon}_{\tilde{3}}(k^*) = 0 \tag{59}$$

The wave vectors are constrained such that $|k_{\tilde{1}}| = |k_{\tilde{2}}| = |k_{\tilde{3}}| = k^*$ and $k_{\tilde{1}} + k_{\tilde{2}} + k_{\tilde{3}} = 0$.

In Figure 6, we show binodal and spinodal ternary diagrams, first for a symmetric polyelectrolyte solution with chain length $N = 100$ and then over a range of polymer lengths. The symmetric polyelectrolyte solution is composed of two identical polymers with opposite linear charge density of 0.15 e/nm and monovalent ions whose volume is 1.5 and solvent volume of 0.03 nm^3. At the quadratic-order level, our explicit treatment of the polar solvent results in a homogeneous dielectric constant dependent on the Debye length that mediates the electrostatic interactions. The polymers have a monomer length and persistence length of 3 nm with a cross-sectional area of 0.1 nm^2. We introduce a polymer–solvent Flory–Huggins parameter $\chi_{PS} = 0.75$, which has the same value for the polycation–solvent and polyanion–solvent. The phase separation shown in this diagram relies entirely on the balance of entropic energy and Flory–Huggins interactions between the solvent ions and polymer since the electrostatics are not included at the mean-field level. On both plots, there is a blue dashed line that is present which indicates the region of interest that is analyzed for the quadratic-order binodals.

Figure 6A includes tie-lines (dotted) that display the connection between the coexistence points along the binodal. Any initial mixture composition that falls on a tie line will phase separate along that line into two phases on the binodal curve. As salt is added to the solution, it starts off equally

https://doi.org/10.1021/acs.macromol.2c01826
Macromolecules 2023, 56, 136–152

distributed between the two phases but is more favorably moved into the supernatant phase as its concentration increases closer to the upper critical point. This behavior arises from the entropic freedom gained within the polymer-lean phase and is independent of polymer length.

The volume fractions of the two polymers and the two ions are combined to maintain that each mixture composition within the ternary diagram is charge neutral. In this formulation, there will always be equal amounts of the two oppositely charged polymers and equal amounts of the two oppositely charged ions. Thus, we are not capturing all the charge-neutral mixture combinations that a polyelectrolyte mixture can take on. The diagram focuses on the effect of adding salt to a polyelectrolyte mixture of equal and oppositely charged polymers. Figure 6B shows the binodal and spinodal curves for six different chain lengths N. The dashed lines show the spinodal curves, where the region between the spinodal curves identifies the unstable conditions for the homogeneous phase. The solid line at the edge of each colored region is the mean-field binodal and represents the coexisting concentrations for the polymer-rich and polymer-lean phases.

A visual analysis of the binodal curves shows that there is a noticeable change in the concavity of the $N = 50$ and 100 curves on the polymer-rich side. This trend exists for all the binodal curves for polymers longer than $N = 25$. The point at which the concavity changes coincides with a constant water volume fraction. For this system, it appears at $\bar{\phi}^{(S)} \approx 0.53$ and matches the critical point of a solution where N goes to infinity.

Starting from the mean-field solutions, we compute the quadratic-order binodal for two different polymer sizes and display the results in Figure 7. For each length, we calculate the quadratic-order chemical potentials using a different approximation of the structure factor to analyze their accuracy for semiflexible polymers. The fluctuations can only be included for the region outside of the spinodal, as the region within the spinodal has nonphysical (negative) fluctuations. Future work will address the fluctuation effects using renormalization group theory, which enables a more systematic analysis of the contributions from concentration and solvent dipole fluctuations. We see that, due to the Flory−Huggins interactions between the polymer and solvent, fluctuations stabilize the disordered phase, resulting in a decrease in the phase separating domain and lowering the upper critical point. The supernatant phase becomes slightly more polymer-rich and the coacervate phase becomes less polymer dense when compared to the mean-field binodal solution.

Due to the symmetry of the polyelectrolyte solution, the binodal solutions shown are also that of an uncharged three-component solution where the ions are treated as point particles and the polymers are thus identical. This also results in the spinodal curve for each of the different chain structure factors being the same. This observation occurs due to the peak fluctuation wave vector coinciding with $\vec{K} = 0$, where the structure factors approach unity for all of the species. Future papers will address the effect of the electrostatics in an asymmetric polyelectrolyte solution where that is not necessarily the case.

At the quadratic-order, the Gauss-rigid model closely captures the correct statistics of the polymers in solution. The largest deviations between the WLC and Gauss-rigid curves appear close to the spinodal where the random phase approximation is less accurate. There is a subtle increase in the difference between the two models as the chain length decreases from $N = 50$ to $N = 10$. This reflects the increasing error in short semiflexible chains at the mesoscale wavevector, shown in Figure 5, that causes a small but noticeable overprediction of the phase-separating domain for the Gauss-rigid model compared to the WLC. The Gaussian chain heavily overpredicts the phase-separating domain because it improperly captures the fluctuations in the high-wavevector regime and is a poor approximation of semiflexible polymers.

CONCLUSIONS

Using a polymer field-theoretical model of polyelectrolyte solutions, we have investigated the effect of different chain structures and polymer lengths on the binodal phase diagrams for a symmetric mixture of oppositely charged polymers in a monovalent salt solution and studied how our explicit dipole treatment modifies the electrostatic potential near a charged surface. Our approach explicitly treats solvent dipole ordering and includes fluctuation corrections to the free energy up to quartic order. While our current analysis of phase behavior focuses on the quadratic-order RPA, our theoretical approach provides a basis for a more systematic analysis of the fluctuation effects in polyelectrolyte solutions.

In the presence of an electric field, the polar solvent molecules undergo a slight reordering away from the salt ions to align more closely with the local electric field. Since the polar solvent molecules act as an effective medium for electrostatic interaction, dielectric inhomogeneity emerges when the solvent is no longer preferably ordered around the ions and the charge−charge interactions are less shielded. The dielectric constant of a polar solvent decreases as the local electric field strength increases, leading to stronger electrostatic interactions. These results indicate the need for dielectric inhomogeneity to be included as they will influence the chain structure of a polymer and become more significant with increasing linear charge density.

For all choices of chain structure, the symmetric polyelectrolyte solution experiences phase separation at near-zero salt concentrations. The symmetry in the system means that the oppositely charged polymers neutralize each other and the counterions can be released, which is not seen in asymmetric mixtures. At high salt concentrations, all of the polyelectrolyte solutions, both symmetric and asymmetric, become homogeneous due to electrostatic screening where the Debye length decreases below the scale of charge interactions. We also show that the upper critical point, which is dominated by salt ions, expectantly increases with polymer chain length due to the decrease in translational entropy.

For a symmetric polyelectrolyte, the choice of chain structure within the RPA formulation heavily dictates the location of the quadratic-order binodal. The binodal for the Gaussian chain overpredicts the phase-separating domain, as it does not accurately capture the fluctuations in the high-wavevector regime. At the quadratic order, the binodal for the Gauss-rigid model closely matches the wormlike chain. Any noticeable deviations between the two models appear close to the spinodal, where the random phase approximation is less accurate. The use of the Gauss-rigid model for quadratic-order fluctuations is viable as a replacement for the wormlike chain model with deviations appearing only at very small polymer lengths. For the cubic and quartic order contributions, however, the wormlike chain model is necessary to accurately capture the solution structure, since the three-point and four-

https://doi.org/10.1021/acs.macromol.2c01826
Macromolecules 2023, 56, 136−152

point structure factor Gauss-rigid approximations cannot be determined from a simple interpolation scheme. At the quadratic order, the explicit treatment of the polar solvent molecules results in an effective homogeneous dielectric constant within the homogeneous solution. Cubic and quartic order corrections are necessary to analyze the effects of dielectric inhomogeneities that are present in polyelectrolyte solutions and will be addressed in a future paper.

APPENDIX A: ELECTROSTATIC POTENTIAL NEAR A CHARGED SURFACE

This section details the calculation of the electrostatic potential near a charged surface developed from eq 27. This mean-field solution is designed to specifically address a monovalent salt water solution with an infinitely long charged surface. The reduction of eq 27 to this simple solution can be accomplished by first removing the polymer terms and noting the exponential form of the ionic contribution in the case of ions with a single valency. Additionally, we replace $\vec{u}$ with $\rho = \cos\theta$ and integrate over all orientations of the dipole, thus removing the θ dependence.

$$\epsilon_0\nabla^2\bar{\psi} = -\frac{q^{(S)}b^{(S)}c^{(S)}}{2}\int d\rho\rho\frac{\partial}{\partial z}\exp\left(\frac{q^{(S)}b^{(S)}}{k_BT}\rho\frac{\partial\bar{\psi}}{\partial z}\right) + 2ec^{(I)}\sinh(e\beta\bar{\psi}) \tag{A.1}$$

The resulting equation is dependent only on the distance away from the charged surface z. Next, we perform an integral over ρ, keeping in mind $\cos\pi = -1$ and $\cos 0 = 1$, and define $A = \frac{q^{(S)}b^{(S)}}{k_BT}\frac{\partial\bar{\psi}}{\partial z}$ to simplify the exponential. We solve the integral by noting that the new form can be created by taking a derivative with respect to A of a generating function, such that

$$\begin{aligned}\int_{-1}^{1} d\rho\rho\,\exp(A\rho) &= \frac{\partial}{\partial A}\left[\int_{-1}^{1} d\rho\,\exp(A\rho)\right]\\ &= \frac{\partial}{\partial A}\left[\frac{1}{A}\exp(A\rho)|_{-1}^{1}\right]\\ &= \frac{\partial}{\partial A}\left[\frac{2\sinh A}{A}\right]\\ &= \frac{2\cosh A}{A} - \frac{2\sinh A}{A^2}\end{aligned} \tag{A.2}$$

The new form of the Poisson equation now looks like

$$\epsilon_0\frac{\partial^2\bar{\psi}}{\partial z^2} = -q^{(S)}b^{(S)}c^{(S)}\frac{\partial}{\partial z}\left(\frac{A\cosh A - \sinh A}{A^2}\right) + 2ec^{(I)}\sinh(e\beta\bar{\psi}) \tag{A.3}$$

Next, we introduce some nondimensionalized terms:

$$\tilde{\psi} = e\beta\bar{\psi}$$

$$\mu = \frac{q^{(S)}b^{(S)}}{e}$$

$$\eta = \frac{z}{z_0}$$

$$A = \frac{\mu}{z_0}\frac{\partial\tilde{\psi}}{\partial\eta}$$

Making the correct replacements we obtain

$$\frac{\epsilon_0}{z_0^2e\beta}\frac{\partial^2\tilde{\psi}}{\partial\eta^2} = -\frac{e\mu c^{(S)}}{z_0}\frac{\partial}{\partial\eta}\left(\frac{A\cosh A - \sinh A}{A^2}\right) + 2ec^{(I)}\sinh\tilde{\psi} \tag{A.4}$$

We then pull out an $A/3$ term from the part inside the first-order derivative to separate out the solvent contribution into its purely dielectric modification, which does not include the orientation effect and a term inside the derivative that does.

$$\frac{\epsilon_0}{z_0^2e\beta}\frac{\partial^2\tilde{\psi}}{\partial\eta^2} = -\frac{e\mu c^{(S)}}{z_0}\frac{\partial}{\partial\eta}\left(\frac{A}{3} + \frac{A\cosh A - \sinh A - \frac{A^3}{3}}{A^2}\right) + 2ec^{(I)}\sinh\tilde{\psi} \tag{A.5}$$

This term can be differentiated out and obtains a second-order derivative of $\tilde{\psi}$ with respect to η.

$$\frac{\epsilon_0}{z_0^2e\beta}\frac{\partial^2\tilde{\psi}}{\partial\eta^2} = -\frac{e^2\mu^2c^{(S)}\beta}{z_0^2e\beta}\frac{1}{3}\frac{\partial^2\tilde{\psi}}{\partial\eta^2} - \frac{e\mu c^{(S)}}{z_0}\frac{\partial}{\partial\eta}\left(\frac{A\cosh A - \sinh A - \frac{A^3}{3}}{A^2}\right) + 2ec^{(I)}\sinh\tilde{\psi} \tag{A.6}$$

We now combine the LHS with the first term on the RHS to explicitly calculate the effective dielectric constant for the medium. It is important to note that this does not obtain the known dielectric constants for most solvents, as there are other interactions like hydrogen bonding that are not included in the model. We define this modified dielectric constant as $\epsilon = \epsilon_0 + e^2\mu^2c^{(S)}\beta/3$, which is the same definition that we used in the quadratic-order fluctuation corrections.

$$\frac{\epsilon}{z_0^2e\beta}\frac{\partial^2\tilde{\psi}}{\partial\eta^2} = -\frac{e\mu c^{(S)}}{z_0}\frac{\partial}{\partial\eta}\left(\frac{A\cosh A - \sinh A - \frac{A^3}{3}}{A^2}\right) + 2ec^{(I)}\sinh\tilde{\psi} \tag{A.7}$$

We then move the coefficients over to the RHS to nondimensionalize the equation.

$$\frac{\partial^2\tilde{\psi}}{\partial\eta^2} = -\frac{e^2\mu c^{(S)}\beta z_0}{\epsilon}\frac{\partial}{\partial\eta}\left(\frac{A\cosh A - \sinh A - \frac{A^3}{3}}{A^2}\right) + \frac{2z_0^2\beta e^2c^{(I)}}{\epsilon}\sinh\tilde{\psi} \tag{A.8}$$

Finally, we define three new nondimensional terms to simplify the expression. We first solve for z_0 by setting the coefficient on the right-most term to 1. This results in $z_0 = l_D = \sqrt{\frac{\epsilon k_BT}{2e^2C^{(I)}}}$ where z_0 solves to be the Debye length. We then introduce $\tilde{\tau} = l_De^2\beta\mu c^{(S)}/\epsilon$ and $\tilde{\mu} = \mu/l_D$, which results in the final expression for the electrostatic potential near a charged surface.

https://doi.org/10.1021/acs.macromol.2c01826
Macromolecules 2023, 56, 136−152

$$\frac{\partial^2\tilde{\psi}}{\partial\eta^2} = \sinh\tilde{\psi} - \tilde{c}\frac{\partial}{\partial\eta}\left[\frac{\tilde{\mu}\frac{\partial\tilde{\psi}}{\partial\eta}\cosh\left(\tilde{\mu}\frac{\partial\tilde{\psi}}{\partial\eta}\right) - \sinh\left(\tilde{\mu}\frac{\partial\tilde{\psi}}{\partial\eta}\right) - \frac{1}{3}\tilde{\mu}^3\left(\frac{\partial\tilde{\psi}}{\partial\eta}\right)^3}{\tilde{\mu}^2\left(\frac{\partial\tilde{\psi}}{\partial\eta}\right)^2}\right] \quad (A.9)$$

APPENDIX B: SOLVENT COUPLING MATRICES

The coupling matrices $M^{(n)}_{\gamma_1\ldots\gamma_n}$ define the terms that appear in the n-order structure factor from the expansion of the solvent partition function.

The expansion of the single-solvent partition function $z^{(S)}$ results in powers of $W_\phi^{(S)}$ and $\vec{W}_D^{(S)}$, but only certain terms survive the integral over the solvent orientation $\vec{u}$. The solvent coupling matrix $M^{(n,S)}_{\gamma_1\ldots\gamma_n}$ is constructed by a factor of $v^{(S)}$ for each power of $W_\phi^{(S)}$ and a factor of $v^{(S)}\vec{u}$ for each power of $\vec{W}_D^{(S)}$ prior to the integration over $\vec{u}$. Only even powers of $\vec{u}$ will survive the orientation integration, resulting in a limited number of coupling terms between $W_\phi^{(S)}$ and $\vec{W}_D^{(S)}$. The $n = 2$ coupling matrix results in two contributions:

$$M^{(2)}_{SS} = 1 \quad (A.10)$$

$$M^{(2)}_{DD} = \langle\vec{u}\vec{u}\rangle = \frac{1}{3}\boldsymbol{I} \quad (A.11)$$

The $n = 3$ coupling matrix results in terms of the form

$$M^{(3)}_{SSS} = 1 \quad (A.12)$$

$$M^{(3)}_{SDD} = M^{(3,S)}_{DSD} = M^{(3,S)}_{DDS} = \langle\vec{u}\vec{u}\rangle = \frac{1}{3}\boldsymbol{I} \quad (A.13)$$

The $n = 4$ coupling matrix results in three types of terms of the form

$$M^{(4)}_{SSSS} = 1 \quad (A.14)$$

$$M^{(4)}_{SSDD} = \langle\vec{u}\vec{u}\rangle = \frac{1}{3}\boldsymbol{I} \quad (A.15)$$

$$M^{(4,S)}_{DDDD} = \langle\vec{u}\vec{u}\vec{u}\vec{u}\rangle \quad (A.16)$$

The term $M^{(4)}_{SDSD}$ (and all other permutations) is equivalent to $M^{(4)}_{SSDD}$. The fourth-rank orientation tensor $\langle\vec{u}\vec{u}\vec{u}\vec{u}\rangle$ is a sparse tensor with only two types of non-zero elements, given by

$$\langle u_z u_z u_z u_z\rangle = \langle u_x u_x u_x u_x\rangle = \langle u_y u_y u_y u_y\rangle = \frac{1}{5} \quad (A.17)$$

$$\langle u_z u_z u_x u_x\rangle = \langle u_z u_z u_y u_y\rangle = \ldots = \frac{1}{15} \quad (A.18)$$

AUTHOR INFORMATION

Corresponding Author

Andrew J. Spakowitz − *Department of Chemical Engineering, Stanford University, Stanford, California 94305, United States; Department of Materials Science and Engineering, Department of Applied Physics, and Biophysics Program, Stanford University, Stanford, California 94305, United States;* orcid.org/0000-0002-0585-1942; Email: ajspakow@stanford.edu

Author

Michael Beckinghausen − *Department of Chemical Engineering, Stanford University, Stanford, California 94305, United States*

Complete contact information is available at: https://pubs.acs.org/10.1021/acs.macromol.2c01826

Notes

The authors declare no competing financial interest.

ACKNOWLEDGMENTS

We are grateful to Jian Qin and Quinn MacPherson for valuable discussions. This work was supported by the NSF program Condensed Matter and Materials Theory, Grant No. 1855334.

REFERENCES

(1) Eghbal, N.; Choudhary, R. Complex Coacervation: Encapsulation and Controlled Release of Active Agents in Food Systems. *LWT* **2018**, *90*, 254−264.

(2) Lan, Y.; Ohm, J.-B.; Chen, B.; Rao, J. Phase Behavior, Thermodynamic and Microstructure of Concentrated Pea Protein Isolate-Pectin Mixture: Effect of pH, Biopolymer Ratio and Pectin Charge Density. *Food Hydrocolloids* **2020**, *101*, 105556.

(3) Li, J.; van Ewijk, G.; van Dijken, D. J.; van der Gucht, J.; de Vos, W. M. Single-Step Application of Polyelectrolyte Complex Films as Oxygen Barrier Coatings. *ACS Appl. Mater. Interfaces* **2021**, *13*, 21844−21853.

(4) Moschakis, T.; Biliaderis, C. G. Biopolymer-Based Coacervates: Structures, Functionality and Applications in Food Products. *Curr. Opin. Colloid Interface Sci.* **2017**, *28*, 96−109.

(5) Butstraen, C.; Salaün, F. Preparation of Microcapsules by Complex Coacervation of Gum Arabic and Chitosan. *Carbohydr. Polym.* **2014**, *99*, 608−616.

(6) Nur, M.; Vasiljevic, T. Can Natural Polymers Assist in Delivering Insulin Orally? *Int. J. Biol. Macromol.* **2017**, *103*, 889−901.

(7) Timilsena, Y. P.; Akanbi, T. O.; Khalid, N.; Adhikari, B.; Barrow, C. J. Complex Coacervation: Principles, Mechanisms and Applications in Microencapsulation. *Int. J. Biol. Macromol.* **2019**, *121*, 1276−1286.

(8) Xiao, Z.; Liu, W.; Zhu, G.; Zhou, R.; Niu, Y. A Review of the Preparation and Application of Flavour and Essential Oils Microcapsules Based on Complex Coacervation Technology. *Journal of the Science of Food and Agriculture* **2014**, *94*, 1482−1494.

(9) Gu, Y.; Zacharia, N. S. Self-Healing Actuating Adhesive Based on Polyelectrolyte Multilayers. *Adv. Funct. Mater.* **2015**, *25*, 3785−3792.

(10) Kobayashi, M.; Terada, M.; Takahara, A. Reversible Adhesive-Free Nanoscale Adhesion Utilizing Oppositely Charged Polyelectrolyte Brushes. *Soft Matter* **2011**, *7*, 5717−5722.

(11) van Hees, I. A.; Hofman, A. H.; Dompé, M.; van der Gucht, J.; Kamperman, M. Temperature-Responsive Polyelectrolyte Complexes for Bio-Inspired Underwater Adhesives. *Eur. Polym. J.* **2020**, *141*, 110034.

(12) Zhang, J.-N.; Zhu, H.; Liu, T.; Chen, Y.; Jiao, C.; He, C.; Wang, H. Strong Adhesion of Hydrogels by Polyelectrolyte Adhesives. *Polymer* **2020**, *206*, 122845.

(13) Bloomfield, V. A.; Wilson, R. W.; Rau, D. C. Polyelectrolyte Effects in DNA Condensation by Polyamines. *Biophys. Chem.* **1980**, *11*, 339−343.

(14) Korolev, N.; Lyubartsev, A. P.; Nordenskiöld, L. Cation-Induced Polyelectrolyte- Polyelectrolyte Attraction in Solutions of DNA and Nucleosome Core Particles. *Adv. Colloid Interface Sci.* **2010**, *158*, 32−47.

(15) Wang, Y.; Gao, T.; Li, S.; Xia, W.; Zhang, W.; Yang, G. Direct Demonstration of DNA Compaction Mediated by Divalent Counterions. *J. Phys. Chem. B* **2019**, *123*, 79−85.
(16) Xiao, F.; Chen, Z.; Wei, Z.; Tian, L. Hydrophobic Interaction: A Promising Driving Force for the Biomedical Applications of Nucleic Acids. *Advanced Science* **2020**, *7*, 2001048.
(17) Strom, A. R.; Brangwynne, C. P. The Liquid Nucleome − Phase Transitions in the Nucleus at a Glance. *Journal of Cell Science* **2019**, *132*, jcs235093.
(18) Brangwynne, C. P.; Tompa, P.; Pappu, R. V. Polymer Physics of Intracellular Phase Transitions. *Nat. Phys.* **2015**, *11*, 899−904.
(19) Durmaz, E. N.; Willott, J. D.; Fatima, A.; de Vos, W. M. Weak Polyanion and Strong Polycation Complex Based Membranes: Linking Aqueous Phase Separation to Traditional Membrane Fabrication. *Eur. Polym. J.* **2020**, *139*, 110015.
(20) Ilyas, S.; de Grooth, J.; Nijmeijer, K.; de Vos, W. M. Multifunctional Polyelectrolyte Multilayers as Nanofiltration Membranes and as Sacrificial Layers for Easy Membrane Cleaning. *J. Colloid Interface Sci.* **2015**, *446*, 386−393.
(21) Magnenet, C.; Jurin, F. E.; Lakard, S.; Buron, C. C.; Lakard, B. Polyelectrolyte Modification of Ultrafiltration Membrane for Removal of Copper Ions. *Colloids Surf., A* **2013**, *435*, 170−177.
(22) Ng, L. Y.; Mohammad, A. W.; Ng, C. Y.; Leo, C. P.; Rohani, R. Development of Nanofiltration Membrane with High Salt Selectivity and Performance Stability Using Polyelectrolyte Multilayers. *Desalination* **2014**, *351*, 19−26.
(23) Aryal, D.; Ganesan, V. Diffusivity of Mono- and Divalent Salts and Water in Polyelectrolyte Desalination Membranes. *J. Phys. Chem. B* **2018**, *122*, 8098−8110.
(24) Muthukumar, M. Double Screening in Polyelectrolyte Solutions: Limiting Laws and Crossover Formulas. *J. Chem. Phys.* **1996**, *105*, 5183−5199.
(25) Castelnovo, M.; Joanny, J.-F. Complexation between Oppositely Charged Polyelectrolytes: Beyond the Random Phase Approximation. *Eur. Phys. J. E* **2001**, *6*, 377−386.
(26) Kudlay, A.; Olvera de la Cruz, M. Precipitation of Oppositely Charged Polyelectrolytes in Salt Solutions. *J. Chem. Phys.* **2004**, *120*, 404−412.
(27) Joanny, J.; Leibler, L. Weakly charged polyelectrolytes in a poor solvent. *J. Phys. (Paris)* **1990**, *51*, 545−557.
(28) Budkov, Y. A.; Kolesnikov, A. L.; Georgi, N.; Nogovitsyn, E. A.; Kiselev, M. G. A New Equation of State of a Flexible-Chain Polyelectrolyte Solution: Phase Equilibria and Osmotic Pressure in the Salt-Free Case. *J. Chem. Phys.* **2015**, *142*, 174901.
(29) Kim, Y. H.; Lee, K.; Li, S. Nucleic Acids Based Polyelectrolyte Complexes: Their Complexation Mechanism, Morphology, and Stability. *Chem. Mater.* **2021**, *33*, 7923−7943.
(30) Rumyantsev, A. M.; Zhulina, E. B.; Borisov, O. V. Scaling Theory of Complex Coacervate Core Micelles. *ACS Macro Lett.* **2018**, *7*, 811−816.
(31) Srivastava, S.; Levi, A. E.; Goldfeld, D. J.; Tirrell, M. V. Structure, Morphology, and Rheology of Polyelectrolyte Complex Hydrogels Formed by Self-Assembly of Oppositely Charged Triblock Polyelectrolytes. *Macromolecules* **2020**, *53*, 5763−5774.
(32) Muthukumar, M. 50th Anniversary Perspective: A Perspective on Polyelectrolyte Solutions. *Macromolecules* **2017**, *50*, 9528−9560.
(33) Sing, C. E. Development of the Modern Theory of Polymeric Complex Coacervation. *Adv. Colloid Interface Sci.* **2017**, *239*, 2−16.
(34) Sing, C. E.; Perry, S. L. Recent Progress in the Science of Complex Coacervation. *Soft Matter* **2020**, *16*, 2885−2914.
(35) Rumyantsev, A. M.; Jackson, N. E.; de Pablo, J. J. Polyelectrolyte Complex Coacervates: Recent Developments and New Frontiers. *Annual Review of Condensed Matter Physics* **2021**, *12*, 155−176.
(36) Voorn, M.*Fortschritte Der Hochpolymeren-Forschung*; Springer, 1959; pp 192−233.
(37) Overbeek, J. T. G.; Voorn, M. J. Phase Separation in Polyelectrolyte Solutions. Theory of Complex Coacervation. *Journal of Cellular and Comparative Physiology* **1957**, *49*, 7−26.
(38) Flory, P. J. Thermodynamics of High Polymer Solutions. *J. Chem. Phys.* **1942**, *10*, 51−61.
(39) Huggins, M. L. Some Properties of Solutions of Long-chain Compounds. *J. Phys. Chem.* **1942**, *46*, 151−158.
(40) Jha, P. K.; Desai, P. S.; Li, J.; Larson, R. G. pH and Salt Effects on the Associative Phase Separation of Oppositely Charged Polyelectrolytes. *Polymers* **2014**, *6*, 1414−1436.
(41) Spruijt, E.; Westphal, A. H.; Borst, J. W.; Cohen Stuart, M. A.; van der Gucht, J. Binodal Compositions of Polyelectrolyte Complexes. *Macromolecules* **2010**, *43*, 6476−6484.
(42) Lee, C.-L.; Muthukumar, M. Phase Behavior of Polyelectrolyte Solutions with Salt. *J. Chem. Phys.* **2009**, *130*, 024904.
(43) Edwards, S. F. The Statistical Mechanics of Polymers with Excluded Volume. *Proceedings of the Physical Society* **1965**, *85*, 613−624.
(44) Edwards, S. F. The Theory of Polymer Solutions at Intermediate Concentration. *Proceedings of the Physical Society* **1966**, *88*, 265−280.
(45) Huang, C.-I.; Lodge, T. P. Self-Consistent Calculations of Block Copolymer Solution Phase Behavior. *Macromolecules* **1998**, *31*, 3556−3565.
(46) Leibler, L. Theory of microphase separation in block copolymers. *Macromolecules* **1980**, *13*, 1602−1617.
(47) Ganesan, V.; Kumar, N. A.; Pryamitsyn, V. Blockiness and sequence polydispersity effects on the phase behavior and interfacial properties of gradient copolymers. *Macromolecules* **2012**, *45*, 6281−6297.
(48) Borue, V. Y.; Erukhimovich, I. Y. A Statistical Theory of Weakly Charged Polyelectrolytes: Fluctuations, Equation of State and Microphase Separation. *Macromolecules* **1988**, *21*, 3240−3249.
(49) Borue, V. Y.; Erukhimovich, I. Y. A Statistical Theory of Globular Polyelectrolyte Complexes. *Macromolecules* **1990**, *23*, 3625−3632.
(50) Sing, C. E.; Olvera de la Cruz, M. Polyelectrolyte Blends and Nontrivial Behavior in Effective Flory−Huggins Parameters. *ACS Macro Lett.* **2014**, *3*, 698−702.
(51) Muthukumar, M. Electrostatic correlations in polyelectrolyte solutions. *Polymer Science Series A* **2016**, *58*, 852−863.
(52) Mahdi, K. A.; Olvera de la Cruz, M. Phase Diagrams of Salt-Free Polyelectrolyte Semidilute Solutions. *Macromolecules* **2000**, *33*, 7649−7654.
(53) Delaney, K. T.; Fredrickson, G. H. Theory of Polyelectrolyte Complexation−Complex Coacervates Are Self-Coacervates. *J. Chem. Phys.* **2017**, *146*, 224902.
(54) McCarty, J.; Delaney, K. T.; Danielsen, S. P. O.; Fredrickson, G. H.; Shea, J.-E. Complete Phase Diagram for Liquid−Liquid Phase Separation of Intrinsically Disordered Proteins. *J. Phys. Chem. Lett.* **2019**, *10*, 1644−1652.
(55) Shen, K.; Wang, Z.-G. Electrostatic Correlations and the Polyelectrolyte Self Energy. *J. Chem. Phys.* **2017**, *146*, 084901.
(56) Qin, J.; de Pablo, J. J. Criticality and Connectivity in Macromolecular Charge Complexation. *Macromolecules* **2016**, *49*, 8789−8800.
(57) Netz, R.; Orland, H. Variational Theory for a Single Polyelectrolyte Chain. *European Physical Journal B - Condensed Matter and Complex Systems* **1999**, *8*, 81−98.
(58) Neugebauer, T. Berechnung der Lichtzerstreuung von Fadenkettenlösungen. *Annalen der Physik* **1943**, *434*, 509−533.
(59) Kratky, O.; Porod, G. Rontgenuntersuchung Geloster Fadenmolekule. *Recl. Trav. Chim. Pay. B* **1949**, *68*, 1106−1122.
(60) Khokhlov, A. R.; Semenov, A. N. Liquid-Crystalline Ordering in the Solution of Long Persistent Chains. *Physica A: Statistical Mechanics and its Applications* **1981**, *108*, 546−556.
(61) Khokhlov, A. R.; Semenov, A. N. Liquid-Crystalline Ordering in the Solution of Partially Flexible Macromolecules. *Physica A: Statistical Mechanics and its Applications* **1982**, *112*, 605−614.
(62) Poitevin, F.; Delarue, M.; Orland, H. Beyond Poisson-Boltzmann: numerical sampling of charge density fluctuations. *J. Phys. Chem. B* **2016**, *120*, 6270−6277.

(63) de Souza, J. P.; Bazant, M. Z. Continuum theory of electrostatic correlations at charged surfaces. *J. Phys. Chem. C* **2020**, *124*, 11414−11421.
(64) Michaeli, I., Overbeek, J., Voorn, M.Phase separation of polyelectrolyte solutions. *J. Polym. Sci.***1957**, *23*, 443.
(65) Booth, F. The Dielectric Constant of Water and the Saturation Effect. *J. Chem. Phys.* **1951**, *19*, 391−394.
(66) Grzetic, D. J.; Delaney, K. T.; Fredrickson, G. H. Contrasting Dielectric Properties of Electrolyte Solutions with Polar and Polarizable Solvents. *Phys. Rev. Lett.* **2019**, *122*, 128007.
(67) Gilson, M. K.; Rashin, A.; Fine, R.; Honig, B. On the Calculation of Electrostatic Interactions in Proteins. *J. Mol. Biol.* **1985**, *184*, 503−516.
(68) Nap, R. J.; Qiao, B.; Palmer, L. C.; Stupp, S. I.; Olvera de la Cruz, M.; Szleifer, I. Acid-Base Equilibrium and Dielectric Environment Regulate Charge in Supramolecular Nanofibers. *Frontiers in Chemistry* **2022**, *10*, 852164.
(69) Budkov, Y. A. Nonlocal Statistical Field Theory of Dipolar Particles in Electrolyte Solutions. *J. Phys.: Condens. Matter* **2018**, *30*, 344001.
(70) Budkov, Y. A. Statistical Theory of Fluids with a Complex Electric Structure: Application to Solutions of Soft-Core Dipolar Particles. *Fluid Phase Equilib.* **2019**, *490*, 133−140.
(71) Budkov, Y. A. A Statistical Field Theory of Salt Solutions of 'Hairy' Dielectric Particles. *J. Phys.: Condens. Matter* **2020**, *32*, 055101.
(72) Budkov, Y. A. Statistical Field Theory of Ion- Molecular Solutions. *Phys. Chem. Chem. Phys.* **2020**, *22*, 14756−14772.
(73) Lamm, G.; Pack, G. R. Calculation of Dielectric Constants near Polyelectrolytes in Solution. *J. Phys. Chem. B* **1997**, *101*, 959−965.
(74) Kanduč, M.; Naji, A.; Jho, Y.; Pincus, P.; Podgornik, R. The role of multipoles in counterion-mediated interactions between charged surfaces: strong and weak coupling. *J. Phys.: Condens. Matter* **2009**, *21*, 424103.
(75) Levy, A.; Andelman, D.; Orland, H. Dielectric constant of ionic solutions: A field-theory approach. *Physical review letters* **2012**, *108*, 227801.
(76) Levy, A.; Andelman, D.; Orland, H. Dipolar Poisson-Boltzmann approach to ionic solutions: A mean field and loop expansion analysis. *J. Chem. Phys.* **2013**, *139*, 164909.
(77) Ma, M.; Xu, Z. Self-consistent field model for strong electrostatic correlations and inhomogeneous dielectric media. *J. Chem. Phys.* **2014**, *141*, 244903.
(78) Koehl, P.; Orland, H.; Delarue, M. Beyond the Poisson-Boltzmann model: modeling biomolecule-water and water-water interactions. *Physical review letters* **2009**, *102*, 087801.
(79) Budkov, Y. A.; Kolesnikov, A. L. Modified Poisson-Boltzmann equations and macroscopic forces in inhomogeneous ionic fluids. *Journal of Statistical Mechanics: Theory and Experiment* **2022**, *2022*, 053205.
(80) Wang, R.; Wang, Z.-G. Inhomogeneous screening near the dielectric interface. *J. Chem. Phys.* **2016**, *144*, 134902.
(81) Koehl, P.; Poitevin, F.; Orland, H.; Delarue, M. Modified Poisson-Boltzmann equations for characterizing biomolecular solvation. *Journal of Theoretical and Computational Chemistry* **2014**, *13*, 1440001.
(82) Martin, J. M.; Li, W.; Delaney, K. T.; Fredrickson, G. H. Statistical field theory description of inhomogeneous polarizable soft matter. *J. Chem. Phys.* **2016**, *145*, 154104.
(83) Kumar, R.; Sumpter, B. G.; Muthukumar, M. Enhanced phase segregation induced by dipolar interactions in polymer blends. *Macromolecules* **2014**, *47*, 6491−6502.
(84) Kumar, R.; Sumpter, B. G.; Kilbey, S. M. Charge regulation and local dielectric function in planar polyelectrolyte brushes. *J. Chem. Phys.* **2012**, *136*, 234901.
(85) Budkov, Y. A.; Kalikin, N. N.; Kolesnikov, A. L. Molecular Theory of the Electrostatic Collapse of Dipolar Polymer Gels. *Chem. Commun.* **2021**, *57*, 3983−3986.
(86) Gordievskaya, Y. D.; Budkov, Y. A.; Kramarenko, E. Y. An Interplay of Electrostatic and Excluded Volume Interactions in the Conformational Behavior of a Dipolar Chain: Theory and Computer Simulations. *Soft Matter* **2018**, *14*, 3232−3235.
(87) Podgornik, R.; Naji, A. Electrostatic disorder-induced interactions in inhomogeneous dielectrics. *EPL (Europhysics Letters)* **2006**, *74*, 712.
(88) Guan, X.; Ma, M.; Gan, Z.; Xu, Z.; Li, B. Hybrid Monte Carlo and continuum modeling of electrolytes with concentration-induced dielectric variations. *Phys. Rev. E* **2016**, *94*, 053312.
(89) Wang, R.; Wang, Z.-G. On the theoretical description of weakly charged surfaces. *J. Chem. Phys.* **2015**, *142*, 104705.
(90) Pryamitsyn, V.; Ganesan, V. Pair interactions in polyelectrolyte-nanoparticle systems: Influence of dielectric inhomogeneities and the partial dissociation of polymers and nanoparticles. *J. Chem. Phys.* **2015**, *143*, 164904.
(91) Grzetic, D. J.; Delaney, K. T.; Fredrickson, G. H. Field-theoretic study of salt-induced order and disorder in a polarizable diblock copolymer. *ACS Macro Lett.* **2019**, *8*, 962−967.
(92) Martin, J. M.; Delaney, K. T.; Fredrickson, G. H. Effect of an Electric Field on the Stability of Binary Dielectric Fluid Mixtures. *J. Chem. Phys.* **2020**, *152*, 234901.
(93) Wang, Z.-G. Effects of Ion Solvation on the Miscibility of Binary Polymer Blends. *J. Phys. Chem. B* **2008**, *112*, 16205−16213.
(94) Samanta, R.; Ganesan, V. Influence of Dielectric Inhomogeneities on the Structure of Charged Nanoparticles in Neutral Polymer Solutions. *Soft Matter* **2018**, *14*, 3748−3759.
(95) Barros, K.; Luijten, E. Dielectric Effects in the Self-Assembly of Binary Colloidal Aggregates. *Phys. Rev. Lett.* **2014**, *113*, 017801.
(96) Zwanikken, J. W.; Olvera de la Cruz, M. Tunable Soft Structure in Charged Fluids Confined by Dielectric Interfaces. *Proc. Natl. Acad. Sci. U. S. A.* **2013**, *110*, 5301−5308.
(97) Jing, Y.; Jadhao, V.; Zwanikken, J. W.; Olvera de la Cruz, M. Ionic Structure in Liquids Confined by Dielectric Interfaces. *J. Chem. Phys.* **2015**, *143*, 194508.
(98) Borukhov, I.; Andelman, D.; Orland, H. Polyelectrolyte solutions between charged surfaces. *EPL (Europhysics Letters)* **1995**, *32*, 499.
(99) Saito, N.; Takahashi, K.; Yunoki, Y. *J. Phys. Soc. Jpn.* **1967**, *22*, 219.
(100) Liu, A. J.; Fredrickson, G. H. Free energy functionals for semiflexible polymer solutions and blends. *Macromolecules* **1993**, *26*, 2817−2824.
(101) Morse, D. C.; Fredrickson, G. H. Semiflexible polymers near interfaces. *Physical review letters* **1994**, *73*, 3235.
(102) Spakowitz, A. J.; Wang, Z.-G. Semiflexible polymer solutions: I. phase behavior and single-chain statistics. *J. Chem. Phys.* **2003**, *119*, 13113−13128.
(103) Chapman, D. L. LI. A contribution to the theory of electrocapillarity. *London, Edinburgh, and Dublin Philosophical Magazine and Journal of Science* **1913**, *25*, 475−481.
(104) Gouy, M. Sur la constitution de la charge électrique à la surface d'un électrolyte. *J. Phys. Theor. Appl.* **1910**, *9*, 457−468.
(105) Molina, C.; Victoria, L.; Arenas, A.; Ibáñez, J. A. Streaming Potential and Surface Charge Density of Microporous Membranes with Pore Diameter in the Range of Thickness. *J. Membr. Sci.* **1999**, *163*, 239−255.
(106) Nakamura, I. Microphase Separation of Ionic Liquid-Containing Diblock Copolymers: Effects of Dielectric Inhomogeneity and Asymmetry in the Molecular Volumes and Interactions between the Cation and Anion. *Macromolecules* **2020**, *53*, 3891−3899.
(107) Wang, R.; Wang, Z.-G. Effects of ion solvation on phase equilibrium and interfacial tension of liquid mixtures. *J. Chem. Phys.* **2011**, *135*, 014707.
(108) Nakamura, I. Spinodal decomposition of a polymer and ionic liquid mixture: Effects of electrostatic interactions and hydrogen bonds on phase instability. *Macromolecules* **2016**, *49*, 690−699.
(109) Wang, Z.-G. Fluctuation in electrolyte solutions: The self energy. *Phys. Rev. E* **2010**, *81*, 021501.
(110) Mao, S.; MacPherson, Q. J.; He, S. S.; Coletta, E.; Spakowitz, A. J. Impact of conformational and chemical correlations on

https://doi.org/10.1021/acs.macromol.2c01826
Macromolecules 2023, 56, 136−152

microphase segregation in random copolymers. *Macromolecules* **2016**, *49*, 4358−4368.
(111) Spakowitz, A. J.; Wang, Z.-G. Exact results for a semiflexible polymer chain in an aligning field. *Macromolecules* **2004**, *37*, 5814−5823.
(112) Spakowitz, A. J.; Wang, Z.-G. End-to-End Distance Vector Distribution with Fixed End Orientations for the Wormlike Chain Model. *Phys. Rev. E* **2005**, *72*, 041802.
(113) Spakowitz, A. J. Wormlike Chain Statistics with Twist and Fixed Ends. *Europhys. Lett.* **2006**, *73*, 684.
(114) Mehraeen, S.; Sudhanshu, B.; Koslover, E. F.; Spakowitz, A. J. End-to-End Distribution for a Wormlike Chain in Arbitrary Dimensions. *Physical Review. E, Statistical, Nonlinear, and Soft Matter Physics* **2008**, *77*, 061803.
(115) Debye, P. Molecular-Weight Determination by Light Scattering. *J. Phys. Colloid Chem.* **1947**, *51*, 18−32.
(116) Chollakup, R.; Beck, J. B.; Dirnberger, K.; Tirrell, M.; Eisenbach, C. D. Polyelectrolyte Molecular Weight and Salt Effects on the Phase Behavior and Coacervation of Aqueous Solutions of Poly(Acrylic Acid) Sodium Salt and Poly(Allylamine) Hydrochloride. *Macromolecules* **2013**, *46*, 2376−2390.
(117) Chollakup, R.; Smitthipong, W.; Eisenbach, C. D.; Tirrell, M. Phase Behavior and Coacervation of Aqueous Poly(Acrylic Acid)-Poly(Allylamine) Solutions. *Macromolecules* **2010**, *43*, 2518−2528.
(118) Li, L.; Srivastava, S.; Andreev, M.; Marciel, A. B.; de Pablo, J. J.; Tirrell, M. V. Phase Behavior and Salt Partitioning in Polyelectrolyte Complex Coacervates. *Macromolecules* **2018**, *51*, 2988−2995.
(119) Lou, J.; Friedowitz, S.; Qin, J.; Xia, Y. Tunable Coacervation of Well-Defined Homologous Polyanions and Polycations by Local Polarity. *ACS central science* **2019**, *5*, 549−557.
(120) Wang, Q.; Schlenoff, J. B. The Polyelectrolyte Complex/Coacervate Continuum. *Macromolecules* **2014**, *47*, 3108−3116.
(121) Neitzel, A. E.; Fang, Y. N.; Yu, B.; Rumyantsev, A. M.; de Pablo, J. J.; Tirrell, M. V. Polyelectrolyte Complex Coacervation across a Broad Range of Charge Densities. *Macromolecules* **2021**, *54*, 6878−6890.
(122) Li, L.; Rumyantsev, A. M.; Srivastava, S.; Meng, S.; de Pablo, J. J.; Tirrell, M. V. Effect of Solvent Quality on the Phase Behavior of Polyelectrolyte Complexes. *Macromolecules* **2021**, *54*, 105−114.
(123) Vieregg, J. R.; Lueckheide, M.; Marciel, A. B.; Leon, L.; Bologna, A. J.; Rivera, J. R.; Tirrell, M. V. Oligonucleotide−Peptide Complexes: Phase Control by Hybridization. *J. Am. Chem. Soc.* **2018**, *140*, 1632−1638.
(124) Rumyantsev, A. M.; de Pablo, J. J. Liquid Crystalline and Isotropic Coacervates of Semiflexible Polyanions and Flexible Polycations. *Macromolecules* **2019**, *52*, 5140−5156.
(125) Lytle, T. K.; Sing, C. E. Tuning Chain Interaction Entropy in Complex Coacervation Using Polymer Stiffness, Architecture, and Salt Valency. *Molecular Systems Design & Engineering* **2018**, *3*, 183−196.

https://doi.org/10.1021/acs.macromol.2c01826
Macromolecules 2023, 56, 136−152